Analysis of 1996 Western American Electric Blackouts

Vaithianathan (Mani) Venkatasubramanian and Yuan Li[1]
School of Electrical Engineering and Computer Science
Washington State University
Pullman WA 99164-2752
Email: mani@eecs.wsu.edu

***Abstract*—**The paper presents a detailed analysis of the 1996 summer blackouts experienced in the western American power system. Computer simulation models are first tuned to match the system responses from wide-area measurements in Pacific Northwest. Power-flow and dynamic analysis show that the July 2, 1996 blackout was caused by reactive power deficiency in the Idaho area, which resulted in voltage instability. Exciter field current limiters likely played a crucial role in pushing the system towards fast voltage collapse. The instability phenomenon of the July 2, 1996 disturbance is shown to be the occurrence of static bifurcations in the power-flow model that led to the loss of steady state equilibrium conditions. Dynamically, the system underwent a saddle node bifurcation and the resulting slow diverging transient was accelerated by further tripping actions that occurred during the event. The fast voltage collapse experienced at Boise and in the Northwest is shown to be related to the singularity of the constrained power system models. Quite unlike the July 2, 1996 blackout, August 10, 1996 blackout is shown to be related to loss of small-signal stability at the equilibrium point. The 0.25 Hz western interarea mode was poorly damped at the start of the event, and it became negatively damped as a consequence of the switching actions that occurred during the disturbance. The western system underwent a Hopf bifurcation on August 10, 1996, which resulted in the growing undamped oscillations. A novel method is proposed for computing unstable limit cycles in large systems. Using this method, a bifurcation diagram is derived for the validated model of the August 10, 1996 western system. The Hopf bifurcation itself is shown to be subcritical, while the interactions of multiple unstable and stable limit cycles influence the phase portraits.

***Keywords*—**Electric blackouts, power system stability, voltage stability, power system dynamics, bifurcations, Hopf bifurcation, saddle node bifurcation, singularity**.**

1. INTRODUCTION

The western electric power grid experienced two major power outages on July 2, 1996 and August 10, 1996 respectively. The first author of this paper was privileged to be an invited member of the industry study group (called the *Operating Capability Study Group*) that was formed to conduct post-mortem studies of these two blackouts. Specifically, the author was actively involved in the duplication of the recorded system responses from a wide-area measurement system that was in place in parts of the Pacific Northwest using computer model simulations. Power-flow conditions just prior to the blackouts, and the wide-area measurements recorded during the disturbances were used to validate the models used in the post-mortem studies. Based on these validated models, the paper will summarize an analysis of the nature of the disturbances. Parts of this paper were included in the model validation reports [1,2] published by the regulatory agency Western Systems Coordinating Council (WSCC) (now called Western Electricity Coordinating council, WECC) in 1997. The reports have since become classified documents. The validation studies were carried out independently by many different companies including the groups at Bonneville Power Administration (BPA) [3,4], Vancouver, WA, Powertech Labs Inc. [5], Surrey, BC, Canada, and at Washington State University. The individual contributions from the different groups formed portions of the model validation reports [1,2]. This paper will summarize the model validation efforts at WSU for the two disturbances as well as the latter analysis of the disturbances using the validated models.

In this paper, we show that the July 2, 1996 blackout was a voltage instability that was caused by loss of steady state equilibrium conditions. Using power-flow models, we show that the disturbance was caused by the system operation being pushed outside the static bifurcation boundary by a double contingency event (Jim Bridger outage). Using dynamic models, we also show that the disturbance was likely caused by the occurrence of a saddle node bifurcation, wherein the initial "slow diverging" trajectory eventually speeds up to a fast voltage collapse, and the acceleration of the voltage decline was caused by the subsequent line and generator trippings. It is interesting that the final fast voltage collapse that eventually led to the system separation along the California-Oregon inter-tie lines appears to have been caused by the behavior of singularity of the power-flow algebraic equations in the constrained dynamic model [6,7,8]. The fast voltage descent (from 0.95 pu to 0.5 pu in 2 seconds) observed at some buses near the Boise region agrees with the dynamic model response following a singularity in the differential-algebraic dynamic model.

[1] Now at Areva TND Corporation, Seattle, WA.

On the other hand, August 10, 1996 blackout was caused by loss of small-signal stability of the operating point caused by some generator trippings and line outages. Using detailed power-flow studies and Prony analysis of small-signal type simulations of validated dynamic models, we show in this paper that the damping of the 0.25 Hz inter-area mode changed from positive to negative values, thus indicating the occurrence of a Hopf bifurcation in the model. Moreover, using a novel method developed at WSU, we compute the location of stable and unstable limit cycles in the large scale validated power system model, and show the complex interaction of the limit cycles in influencing the oscillatory nature of the disturbance. Specifically, we show that the Hopf bifurcation itself was likely a subcritical Hopf bifurcation associated with unstable limit cycles, while the eventual system separation was likely caused by the annihilation of a stable limit cycle at a cyclic fold global bifurcation. These results on the August 10, 1996 blackout formed a portion of the 2003 doctoral dissertation [9] of the second author of this paper at WSU.

The paper is organized as follows. The discussion of the July 2, 1996 blackout is presented in Section 2. The mechanisms of the August 10, 1996 event are analyzed in Section 3 using the validated dynamic models.

2. ANALYSIS OF JULY 2, 1996 WESTERN ELECTRIC DISTURBANCE

An excellent summary of the July 2, 1996 blackout can be seen in pages 22 to 30 of Reference [10] published by North American Electric Reliability Council (NERC). A one-line diagram of the key buses that participated in the disturbance is presented in Figure 1.

The event was initiated at 2.24 PM PST by a routine fault on the 345 kV transmission line between Jim Bridger and Kinport which was opened by system protection. Because of relay misoperation, the adjacent 345 kV line connecting Jim Bridger to Goshen also was tripped shortly thereafter. Therefore, two of the three 345 kV lines that export power out of the Jim Bridger power plants were tripped out of service, and the resulting power-flow was infeasible by itself. To correct the situation, a remedial action scheme (RAS) was triggered by the RAS controller. The RAS scheme included 1) tripping two of the four Jim Bridger units (about 1040 MW), 2) bypassing the series capacitors at two nearby transmission lines and 3) inserting a 175 MVAR shunt capacitor bank at Kinport.

Under normal circumstances, the RAS scheme should have stabilized the system following the double outage of the two 345 kV transmission lines out of Jim Bridger. However, on July 2, 1996, the voltages started declining slowly in the Boise area (including Kinport, MidPoint, Boise etc.) even after the switching of the RAS scheme, and several small generators in the area and some of the lower voltage transmission lines tripped in the period of 20 seconds following the RAS action. These trippings will be discussed in more detail a little later on.

At about twenty seconds following the initiating event, the 230 kV transmission line connecting Antelope and Anaconda (the Amps line) tripped because of a Zone 3 relay. Within a few seconds after the loss of the Amps line, the voltage at the 230 kV load bus Boise dropped dramatically from about 210 kV to 150 kV in a span of about three seconds. Around that time, the four Boise Bench 230 kV lines connecting Brownlee and Boise tripped which appeared to quickly trigger the blackout. Within two seconds after the tripping of the Boise Bench lines, the voltage at the 500 kV Malin bus on the California-Oregon AC tie-lines (COI) collapsed to around 300 kV. The low voltages led to the tripping of the COI lines that resulted in system separation and the widespread blackout in the western electric grid. The actual voltage recordings at the Boise 230 kV bus and the Malin 500 kV bus are shown in Figure 2.

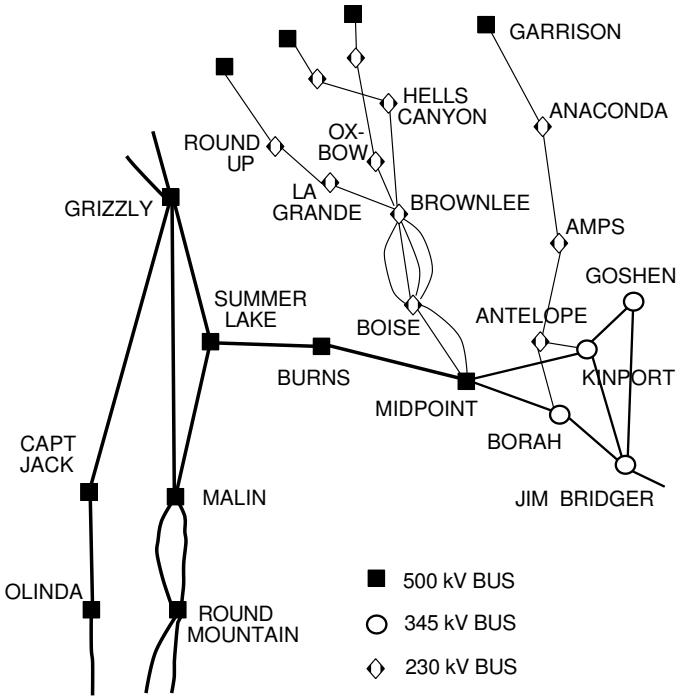

Figure 1. One-line diagram of the key buses related to the July 2, 1996 event

It is significant that the system had separated within thirty seconds after the initiating fault on the Jim Bridger-Kinport line. Such a short time of less than thirty seconds prevented the possibility of any operator intervention. Also, the fast voltage declines which occurred within the Idaho area and on the COI lines (Figure 2) had not been encountered earlier in real power systems. We will first summarize power-flow analysis of the system conditions in Section 2.1. We show that *the western power system was power-flow infeasible after the double Bridger contingency even after taking into account the RAS scheme.* The infeasibility becomes gradually more severe as further trippings occur. *On July 2, 1996, the system was operating well outside the static bifurcation boundary when the eventual system separation occurred.*

Next, we will present model validation results of the time-domain simulations in Section 2.2. It is interesting that the fast voltage declines were captured reasonably well in our

validated models, and the simulation results matched quite well with actual system recordings. In Section 2.3, we will carry out an analysis of the nature of the disturbance from time-domain simulations of the validated model. We will see that *the system underwent a saddle node bifurcation that annihilated the normal equilibrium type operating condition.* The resulting diverging slow transient is accelerated by further trippings that speed up the voltage decline. And, the system gets pushed into the proximity of the singularity [6,8] or the non-causality [7] of the differential-algebraic equations (DAE). Based on our simulations, we postulate that *the spectacularly fast voltage collapse at Boise and later on the COI buses was caused by the DAE singularity of the constrained power system.*

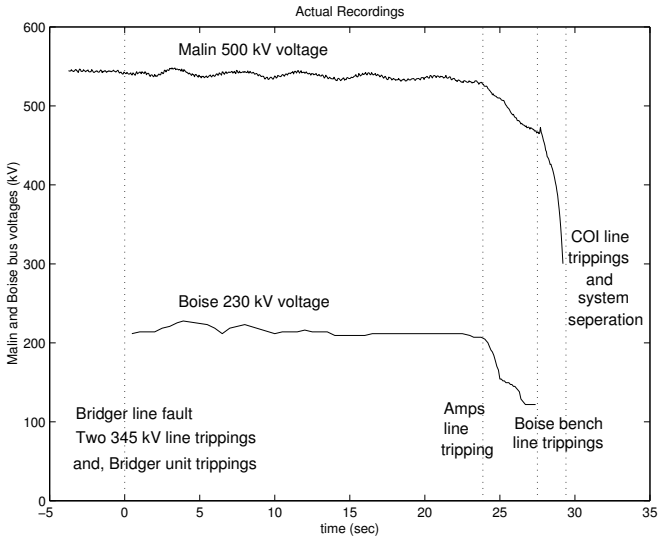

Figure 2. Recordings of key bus voltages

2.1. Power-flow studies:

This report discusses power-flow studies of the WSCC power-flow case 2jul6d.net which represents the power-flow conditions of the WSCC system at 2.24 PM PST on July 2, 1996, just prior to the initial fault occurrence on the Jim Bridger-Kinport line. All the studies were carried out using the EPRI power-flow program IPFLOW. For the case 2jul6d.net, the system had negative VAR margin after the double Bridger unit outage, apparently because of reactive power deficiency in the Idaho area. The VAR deficiency becomes more severe when additional lines and generation units are tripped along the sequence of events as they occurred during the July 2nd event. The first author the paper thanks Mr. Parthasarathi Nag at WSU for his help with the power-flow studies in this section.

2.1.1. Post-transient power-flow studies:

The objective of the study is to assess the reactive power margins of the power-flow base case 2jul6d.net along the sequence of events as they occurred on the July 2, 1996 disturbance.

2.1.1.1 Reactive power margin study:

Post-transient power-flow analysis of the following seven cases were studied first for quantifying the reactive margins at various stages of the event. The sequence of switchings shown below matches the switching sequence during the July 2nd disturbance.

Case A: Base case power-flow 2jul6d.net.
Case B: Bridger to Kinport 345 kV line is tripped.
Case C: Case B is extended by tripping Bridger to Goshen 345 kV line. Bridger units 2 and 4 are tripped. 175 MVAR shunt compensation is switched in at Kinport, and series capacitors are bypassed on Bridger to Borah 345 kV line, and Summer Lake to Burns 500 kV line.
Case D: Case C is extended by tripping La Grande to Round-up 345 kV line.
Case E: 59 MVAR shunt compensation is switched in next at the Anaconda 230 kV bus.
Case F: Strike generation is tripped.
Case G: Lucky Peak generation is tripped.
Case H: Antelope to Anaconda 230 kV line (Amps line) is tripped.

During the July 2nd disturbance, the Boise voltage declined rapidly following the tripping of the Amps line. This in turn led to the tripping of Boise bench lines and to the collapse of the COI bus voltages. Therefore, power-flow analysis was carried out up to the tripping of the Amps line to understand the power-flow conditions up to and after the tripping of the Amps line.

All the controls were enabled for the base case power-flow solution. For the post-transient studies from Cases B through H, generator and SVC controls were enabled, while tap changers and shunt compensation devices were locked at the pre-contingency values. Preliminary power-flow studies indicated that there was no valid power-flow solution for Case C, after the tripping of two Bridger lines and two Bridger units. There does exist a spurious power-flow solution when the generator reactive limits are deactivated, and the reactive power outputs of several generators in the Idaho area are well above their steady state VAR limits in the spurious solution. This clearly establishes that there exists a VAR deficiency problem in the Idaho area for getting a valid Case C power-flow solution.

To study the reactive power deficiency, switching of fictitious capacitor banks was studied at various buses near the Jim Bridger plants and the rated values of the capacitors were varied to compute the Q-V plot at each of the buses. Among the 500 kV lines in the area, Mid Point bus is seen to be a sensitive bus and the reactive power margin to the nose point (static limit) of the Q-V plot is -275 MVAR at Mid Point. The VAR margin for a Q-V plot at Borah 345 kV bus is about –410 MVAR, and the other buses in the area have slightly more negative VAR margins. On the other hand, the VAR margin at Malin is about –800 MVAR, which clearly indicates that

Malin 500 kV bus is electrically far away from the VAR deficiency area.

Among the 230 kV buses, Boise and Brownlee buses were among the most sensitive buses. The Q-V plots for reactive power variation at Boise and Brownlee are shown below. The VAR margins at Boise and Brownlee are -140 MVAR (Figure 3) and -170 MVAR (Figure 4) respectively.

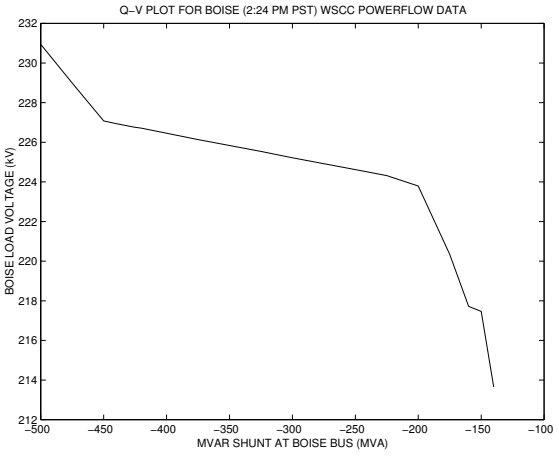

Figure 3. Post-transient QV plot at Boise 230 kV bus

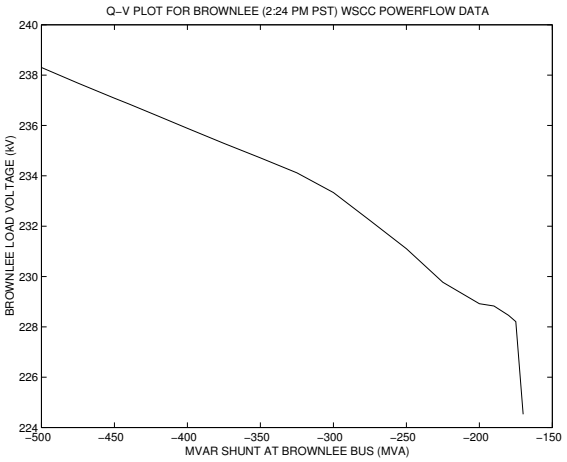

Figure 4. Post-transient QV plot at Brownlee 230 kV bus

As a clarification, note that a negative margin of -140 MVAR at Boise for Case C implies that a minimal additional shunt compensation of 140 MVAR at Boise bus is needed for getting a valid power-flow solution for Case C. The minimum capacitive support needed at the Brownlee bus is then 170 MVAR. These two margins are the lowest among the margins at various buses in the area. Therefore, *we conclude the buses Boise and Brownlee are the critical buses for the reactive power deficiency after the two Bridger line outage contingency, that is, for Case C power-flow.*

Next, we will study the severity of the reactive power deficiency as the switching events progressed during the July 2nd event. The listing of switchings is provided in the form of Case A through Case H at the beginning of this subsection. To study the VAR deficiency problem, two fictitious capacitor/reactor banks of equal value were switched in at Boise and Brownlee buses, and their values were varied to compute Q-V plots for Cases A through H. When shunt compensation at only one of the two buses either Boise or Brownlee was considered, the capacitor bank values required for getting valid solutions were rather high. Therefore, shunt compensation of equal value at both Boise and Brownlee buses was studied.

Under the variation of VAR shunt at Boise and Brownlee, the margins to the nose of the Q-V plots for each of the cases are summarized below. Since the shunt compensation at *both* Boise and Browlee are being varied, the QV margin at any of these two buses would be roughly *twice* the values shown below.

Case A: (base case): Margin is +145 MVAR (Figure 5)
Case B: (Bridger to Kinport open): Margin is +110 MVAR (Figure 6)
Case C: (Two Bridger line outage contingency): Margin is -70 MVAR (Figure 7)
Case D: (La Grande to Round-up Open): Margin is -75 MVAR (Figure 8)
Case E: (Anaconda cap switched in): Margin is -60 MVAR (Figure 9)
Case F: (Strike units dropped): Margin is -115 MVAR (Figure 10)
Case G: (Lucky Peak units dropped): Margin is -150 MVAR (Figure 11)
Case H: (Amps line tripped): Margin is –170 MVAR (Figure 12)

The reactive margin changes from positive to negative right after the initiating event namely the tripping of two Bridger lines and the associated RAS scheme.

The Q-V plots for Cases A and B are discussed first. Before the contingency, the VAR margin for the base case is seen to be about +145 MVAR (Figure 5). The margin drops to about +110 MVAR after the tripping of the Bridger to Kinport 345 kV line in Case B (Figure 6). During the July 2nd disturbance however, because of incorrect relay operation, the parallel line Bridger to Goshen 345 kV line was also tripped thus leading to the Case C scenario.

The system is significantly reactive power deficient in Case C (Figure 7) with a VAR margin of -70 MVAR for shunt compensation each at the Boise and Brownlee buses. The tripping of the parallel line (Bridger to Goshen line) and the associated remedial actions have severely impacted on the reactive demands in the area. For a Case C power-flow solution on the Q-V plot below near the static limit, it is seen that the generators in the Idaho area are operating at their steady state VAR limits which again points to reactive power problems in the area. On the other hand, the VAR outputs of the Jim Bridger plants are below their reactive power limits.

Note that after the tripping of the two 345 kV lines out of the Bridger plant, the two remaining Bridger units are operating in a single-machine-infinite-bus like configuration towards Idaho, and hence the Bridger units are somewhat electrically isolated from the voltage support problems in the area.

Next, when the La Grande to Round-Up 230 kV line is tripped, the VAR margin drops to -75 MVAR for Case D (Figure 8). The switching of 59 MVAR capacitor bank at Anaconda improves the reactive deficiency in the area somewhat, and the margin for Case E is -60 MVAR (Figure 9).

In other words, the Q-V plot above implies that a minimal additional capacitive shunt compensation of at least 175 MVAR is necessary at each of Boise and Brownlee buses for getting a valid power-flow solution after the tripping of the Amps line. Owing to this severe reactive power deficiency, the Boise voltage collapsed rapidly following the Amps line tripping during the actual event.

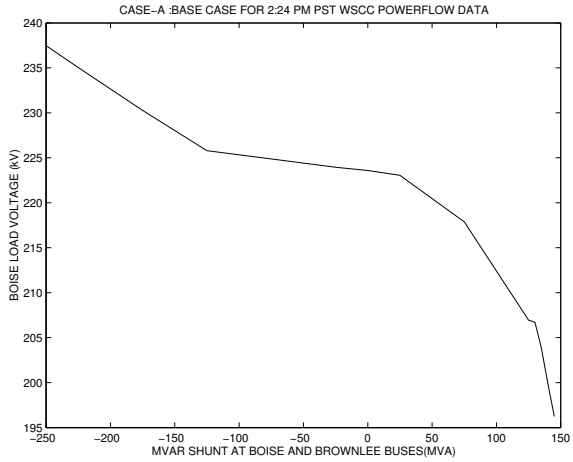

Figure 5. QV plot for Case A power-flow conditions

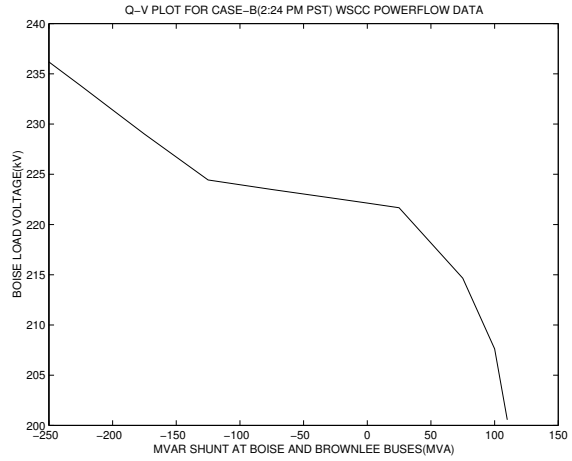

Figure 6. QV plot for Case B power-flow conditions

The next switching event was the tripping of Strike units, which reduces the VAR margin to -115 MVAR (Figure 10). Note the significant change in the VAR margin with the tripping of the Strike units. In the time-domain simulation studies that follow later in Section 2.2, we will see that the tripping of the Strike units might have been crucial in pushing the system towards the voltage collapse. The tripping of Lucky Peak generator further reduces the VAR margin to about -150 MVAR for Case G (Figure 11).

From these Q-V plots, it is very clear that the system was becoming more and more reactive power deficient as the switching sequence progresses. Next, when the Amps line is tripped, the system appears to be severely reactive deficient, and the negative VAR margin grows to –175 MVAR in Figure 12.

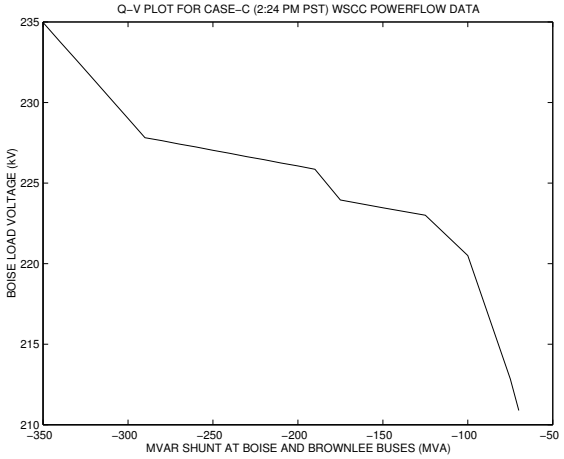

Figure 7. QV plot for Case C power-flow conditions

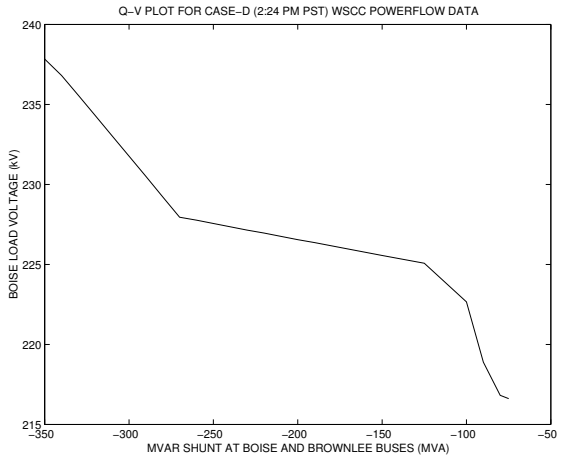

Figure 8. QV plot for Case D power-flow conditions

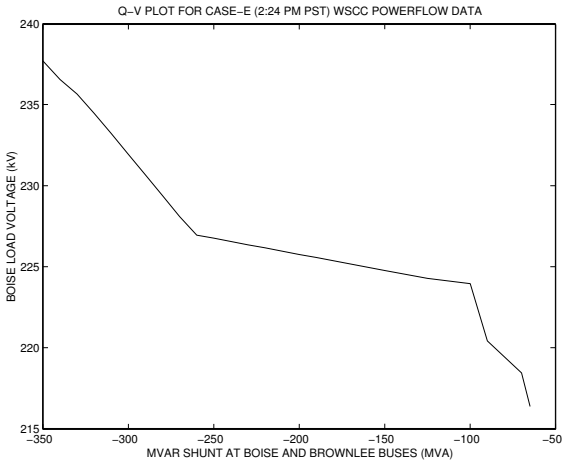

Figure 9. QV plot for Case E power-flow conditions

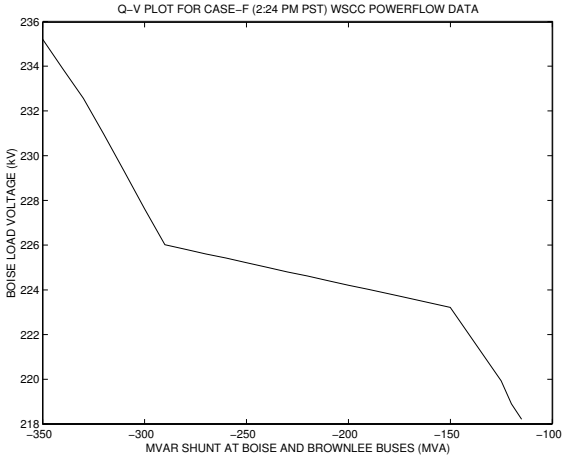

Figure 10. QV plot for Case F power-flow conditions

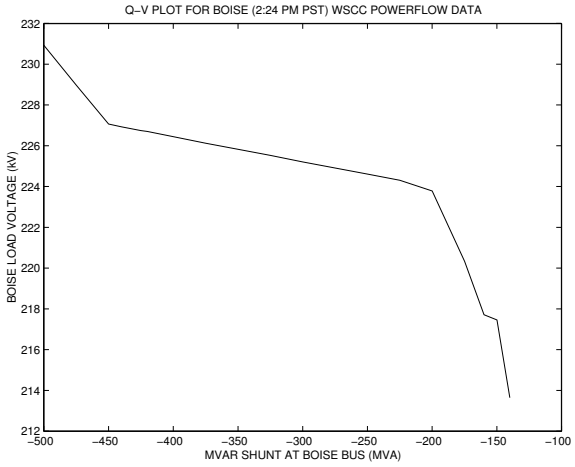

Figure 11. QV plot for Case G power-flow conditions

In general, power-flow studies such as the one presented above are typically conservative in modeling the reactive resources of the system since all the loads are represented here by constant MVA loads, and the steady state VAR limits of generators are also modeled rather conservatively. During typical transient time-periods after fault clearings, generators can provide much larger reactive power support than their steady state VAR limits. Therefore, reactive power deficiency in the power-flow study while it shows voltage insecurity may not explain the fast voltage collapse, which occurred within thirty seconds after the initiating contingency during the July 2nd event. However, the progressively more severe nature of the reactive power deficiency in the Idaho area as shown in this study along the switching sequence, clearly shows that the system was becoming more and more stressed for voltage support as the event progressed. This increasing severity of reactive deficiency along the switching sequence definitely indicates the occurrence of a voltage collapse scenario.

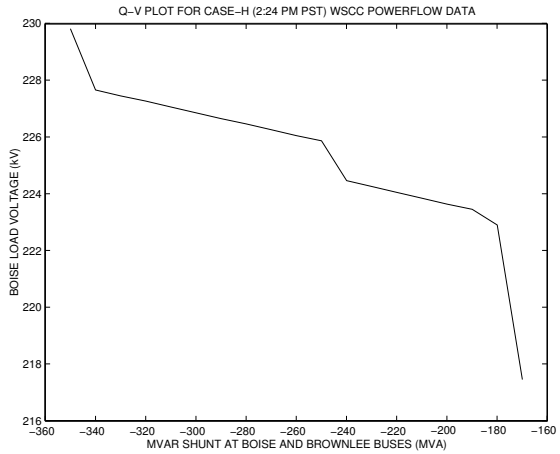

Figure 12. QV plot for Case H power-flow conditions

In the time-domain simulation to be presented in a separate section, we will see that the Boise bench condenser and the Brownlee generator in the Idaho area are operating above their steady state field current limits right after the initiating event, namely, the two Bridger line tripping contingency. The field currents surge as the switching sequence progresses since the reactive power demands are becoming more and more severe. Eventually, the field over-current limiters become active in the simulation at Boise bench and Brownlee right after the tripping of Amps line. Once the field current limiters become active at Boise bench and Brownlee, the reactive power output of the two units decrease to values near their steady state VAR limits, and the Boise voltage collapses rapidly owing to the severity of the reactive power deficiency. The power-flow studies of this section are therefore very much consistent with the time-domain analysis of the disturbance to be presented later in Section 2.2.

2.1.2 Sensitivity to series capacitor by-pass:

The remedial actions following the tripping of the two Bridger lines during the July 2nd event included the bypassing of series capacitors on Summer Lake to Burns 500 kV line, and Bridger to Borah 345 kV line. In Section 2.1.1, the Q-V study showed the VAR margin to be -140 MVAR for shunt VAR variation at Boise bus. When the series capacitors are in service, there does exist a valid power-flow solution after the Bridger two-

line outage contingency, and the VAR margin is about +10 MVAR at Boise. After the bypassing of the series capacitors, the VAR margin becomes significantly negative -140 MVAR at Boise. The series capacitor by-pass action appears to have partially contributed to the reactive power deficiency in the area. If the series capacitors are in service, the area voltages are also higher, and therefore, the line currents are lower for the power-flow solution. Therefore, the chances of cascading line trippings and generation trippings might have been lower with the series capacitors in service during the disturbance. However, if the tripping sequence proceeds as they occurred during the July 2nd event, the reactive margin becomes negative after the tripping of the La Grande to Round Up 230 kV line, even if the series capacitors on the two lines had been in service. These observations are also consistent with the time-domain sensitivity study, which is presented separately.

2.1.3 Sensitivity to shunt compensation at Malin 500 kV bus:

There are two capacitor banks rated at 216 MVAR each, stationed at the Malin 500 kV bus on the California-Oregon border which are switched in to provide reactive support to the California-Oregon tie-lines when the Malin voltage falls below certain pre-set values. In this study, the VAR support at Malin bus is related to the VAR deficiency in the Idaho area. Recall that the reactive margin for Case C was computed in Section 2.1.1 to be –70 MVAR at Boise and Brownlee buses. For the study below, the two capacitor banks at Malin are assumed to be switched in, and the Q-V plot for Case C is recomputed. The VAR margin with 400 MVAR capacitive support at Malin is recomputed to be about -65 MVAR (Figure 13), whereas the VAR margin was previously at -70 MVAR with no capacitive support at Malin. In other words, switching of 400 MVAR shunt compensation at Malin does not affect much the reactive power deficiency in the Idaho area for Case C. This is clear also from the system topography since Malin is electrically far away from the critical Idaho buses. It is well-known in literature that reactive power issues need to be addressed locally near the problem areas. Owing to the inherent inductive nature of the transmission lines, capacitive reactive power cannot be "transmitted" over long transmission paths. The study suggests that the reactive power problems were first dominant in the Idaho area (near the Boise bus). The voltage collapse then later spread to Malin, and not vice versa.

2.1.5 Sensitivity to Boise load:

In Section 2.1.1, it was shown that the power-flow case is reactive power deficient for Case H, that is, after Amps line tripping, and an additional shunt compensation of about 180 MVAR each at Brownlee and Boise bench buses is necessary for getting a valid power-flow solution for the Case H scenario. As an alternate remedial control measure, shedding of a portion of the Boise load is studied in this subsection again for the Case H scenario after the tripping of the Amps line. If 20% of Boise load is tripped, then the VAR margin at Boise can be computed by Q-V analysis to be –130 MVAR. In other words, when 20% of Boise load is tripped, an additional capacitor support of at least 130 MVAR is necessary at each of Boise and Brownlee buses for getting a valid Case H power-flow solution. Next, if 30% of the Boise load is tripped, the VAR margin improves to –50 MVAR. When 40% of Boise load is tripped under Case H operating conditions, the VAR margin improves to a small positive reactive power margin of +5 MVAR at Boise and Browlee (Figure 14). A valid power-flow solution exists for the case 2jul6d even after the tripping of Amps line if 40% of Boise load is tripped under these conditions.

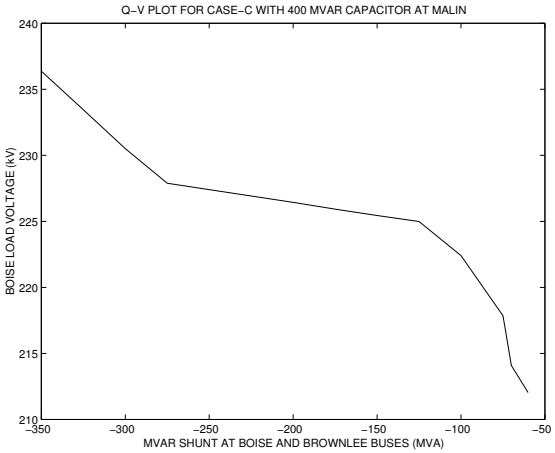

Figure 13. QV plot for Case C after switching in +400 MVAR at Malin

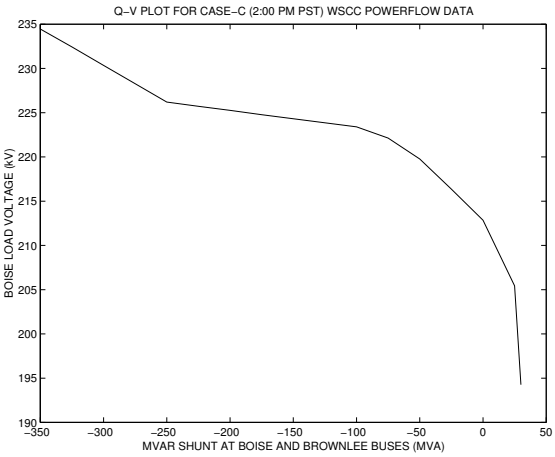

Figure 14. QV plot for Case H after 40% load shedding at Boise

2.1.6 Power-flow feasibility studies:

The concept of power-flow feasibility regions was proposed by Galiana et. al. in [11] for understanding the proximity of an operating condition to static limit boundaries. In this subsection, we will study the power-flow feasibility region under variations in the real and reactive power loads at the Boise bus. Figure 15 summarizes the feasibility region and the infeasibility boundary for the base case power-flow scenario Case A. Noting that the actual loads at Boise were about 530 MW and about 300 MVAR at the start of the disturbance, it is

easily seen that the system operation is well-within the feasibility boundary for Case A. Since the power-flow equations represent the steady state equilibrium solutions of the power system, the feasibility boundary in Figure 15 corresponds to the static bifurcation boundary in the sense of nonlinear system theory. There exist no valid power-flow solutions on the infeasible side of the feasibility boundary in Figure 15. This is consistent with the occurrence of static fold bifurcations or the static versions of the saddle node bifurcations along the feasibility boundary in Figure 15.

A direct comparison of the feasibility boundaries for Cases A, C and H is presented in Figure 16. Here, it is easily seen that the actual conditions were inside the boundary in Case A. The operating conditions were infeasible for Case C and the infeasibility becomes a lot more severe for Case H.

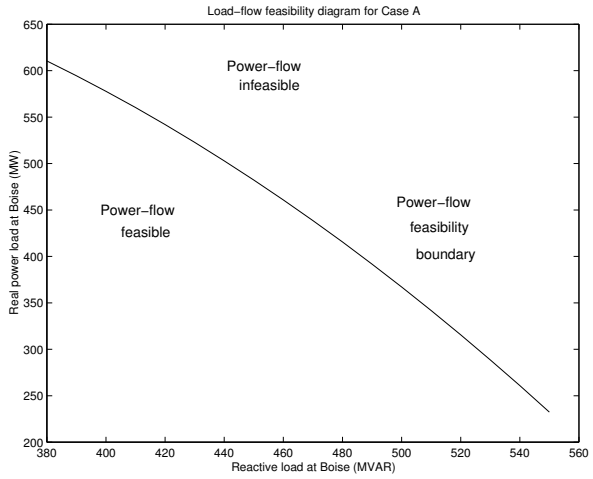

Figure 15. Power-flow feasibility diagram for Case A

In power system literature [12], it is well known that proximity of system operating conditions to the static bifurcation boundary or the feasibility boundary can lead to voltage collapse problems. In this case, we see next that the actual load conditions at Boise were outside the feasibility boundary in Case C (Figure 16) after the double Bridger line outage contingency. In other words, the tripping of the two 345 kV lines out of Jim Bridger and the subsequent RAS scheme switchings have pushed the system operation from "well inside" the feasibility region in Case A to outside the feasibility boundary in Case C. The double Jim Bridger outage has thus rendered the system operation infeasible in the power-flow sense in Case C in Figure 16. Again, for Case H, and clearly, the operating conditions have moved further outside the feasibility boundary in Figure 16.

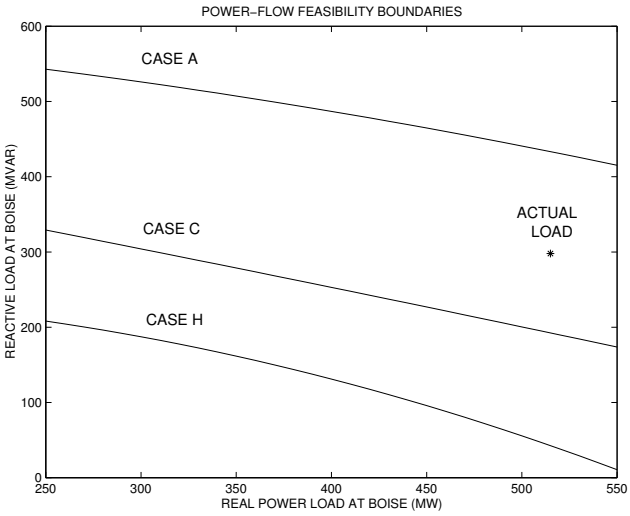

Figure 16. Comparison of the power-flow feasibility regions

2.1.7 Summary of the power-flow studies:

The detailed power-flow studies of the consequences of the switching sequence during the July 2, 1996 event have shown that the Idaho subsystem experienced reactive power deficiency that became gradually more severe as the trippings progressed. The system was operating outside the feasibility boundary after the initial double Bridger outage and the RAS scheme did not make the operation feasible for those power-flow conditions. *Power-flow results in this section clearly establish that the system operation was pushed outside the static bifurcation boundary by the switchings that unfolded during the disturbance.* Power-flow sensitivity studies showed that insertion of two 500 kV Malin capacitor banks near the COI lines would not have helped the reactive deficiency in the Idaho region. The studies also indicate that the reactive power problems in Idaho could have been mitigated by tripping of about 40% of the Boise load.

2.2. Time-domain simulation results:

The time-domain behavior of the July 2nd event has been largely captured in ETMSP based transient stability analysis by extending the WSCC base case model data in three aspects: 1) modeling of excitation limiters on critical Idaho generators in the Boise area, 2) modeling of nonlinear dynamic load models in the Idaho area, and 3) blocking of governors in all those thermal units in the WSCC system that have generations above 100 MW. ETMSP simulations of various bus voltages during the event closely follow the actual BPA and Idaho time recordings of bus voltages in the Boise area and on the COI inter-tie. The frequency behavior of the July 2nd event is also closely duplicated in the simulations.

Time recordings from the event as well as numerical simulations indicate that the system was operating under heavily stressed yet possibly in a marginally stable condition just after the initial sequence of line trippings and Bridger unit drops. During the 24 seconds after the initiating sequence of Bridger

trippings, the COI inter-area mode at 0.25 Hz had near zero damping which led to poorly damped oscillations of COI voltages and power-flows. Moreover, after the Bridger unit trippings, the generators in the Boise area appear to have been operating under heavily stressed condition near or above their steady state VAR limits. After the tripping of several small generators in the Idaho area and with the Amps line tripping, there appears to have been insufficient dynamic VAR support for sustaining stable power-flows in the Idaho area, which appears to have caused the rapid voltage collapse in the Boise region. After the two Bridger line trippings, the Jim Bridger plants were operating in a single-machine-infinite-bus like configuration and voltage support along the Mid Point to Summer Lake 500 kV tie was limited.

2.2.1. ETMSP simulations of the July 2, 1996 event:

This section summarizes a comparison of transient stability simulations on EPRI transient stability program ETMSP using various sets of model cases and the actual time-recordings. In these simulations, minor enhancements of the base case data, as detailed below, resulted in a close matching of the simulations with some of the main features of the actual time-recordings.

One of the main characteristics of the July 2nd event was the rapid voltage decline in the Idaho area immediately after the Amps line tripping that led to the tripping of Boise bench lines, which in turn accelerated the decline of the COI bus voltages. Prior to the Amps line tripping, there also was a gradual decline of the COI bus voltages (about 3% over 23 seconds) together with low amplitude poorly damped 0.25 Hz oscillations. During this period, the power-flows on the COI lines were gradually recovering (about 400 MW over 23 seconds) and the COI voltages appeared to be adjusting to lower values possibly associated with the different power-flows. The Tacoma frequency dipped to about 59.86 Hz (which was caused by the Jim Bridger generation loss) within 6 seconds after the Bridger unit trippings while it accelerated to about 60.40 (which was caused by low voltage related loss of loads) after Amps and Idaho line trippings, just before the inter-tie separation.

The power-flow case 2jul6d.net used in these validation studies matches the power-flow characteristics of the WSCC system at the starting time-instant 14.24 PM PST of the July 2nd disturbance event. The machine exciter data of a few generators in the base case stability data was first modified to fix certain spurious local oscillations in the simulations, which were apparently caused by bad data. Next, a transient stability simulation of the July 2nd event switching sequence was carried out using this base case stability data and the power-flow case 2jul6d. Time-plots for Malin and Boise bus voltages from the simulations in Figures 17 and 18 respectively, do not show voltage stability problems in Idaho and Northwest after the tripping of Bridger units, and hence the simulations are not consistent with the system behavior during the disturbance.

A closer inspection of the generator field voltages, field currents and VAR outputs in the Idaho and BPA areas revealed that the filed outputs of the units in the Boise area (specifically the Boise bench condenser and the Brownlee generators in Figures 19 and 20) are unrealistically large during this voltage recovery of the simulations.

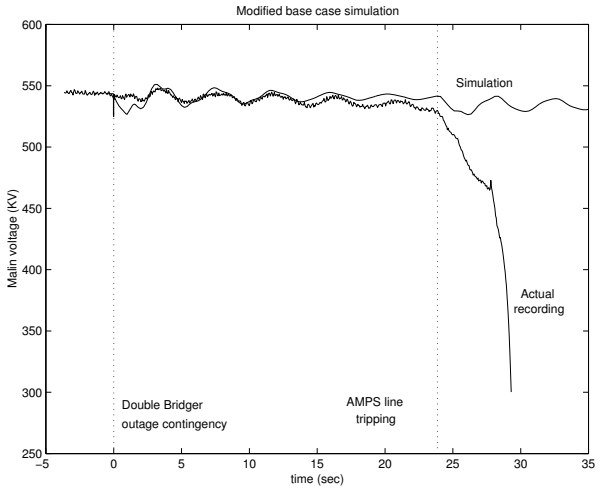

Figure 17. Malin bus voltage time-plot

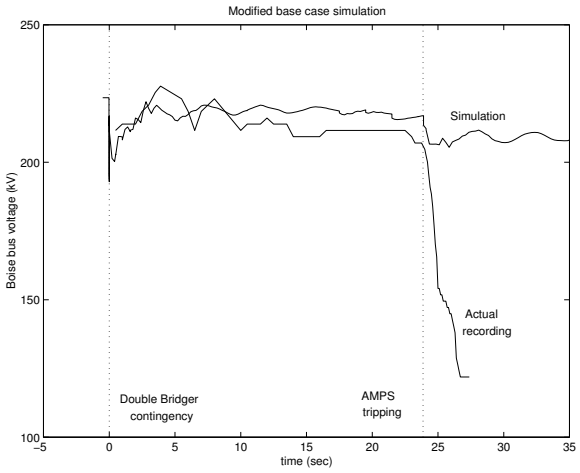

Figure 18. Boise bus voltage time-plot

Therefore, to model the dynamic VAR outputs of the Idaho units in a more realistic fashion, field over-current limiters were introduced in the simulation model for the Idaho units near Boise. Ron Schellberg at Idaho Power Company provided the values for these limiters. When the field current limiters are modeled at Boise Bench and Brownlee units, the voltage collapse of the Boise area voltages and of the COI voltages can be seen in the simulations shown below. After the initial sequence of line trippings and Bridger unit trippings, these two units (and some other smaller generators in the area) are operating above their steady state VAR limits in the simulations. With the tripping of Lucky Peak generator and with Amps line tripping, field currents surge on these in trying to adjust to increased power-flows which activate the over-

current limiters at Boise Bench and Brownlee in the simulation. After the two Bridger line trippings, the Jim Bridger units appear to be operating in a single-machine-infinite-bus like configuration and the voltage support along the Mid Point to Summer Lake 500 kV tie is limited.

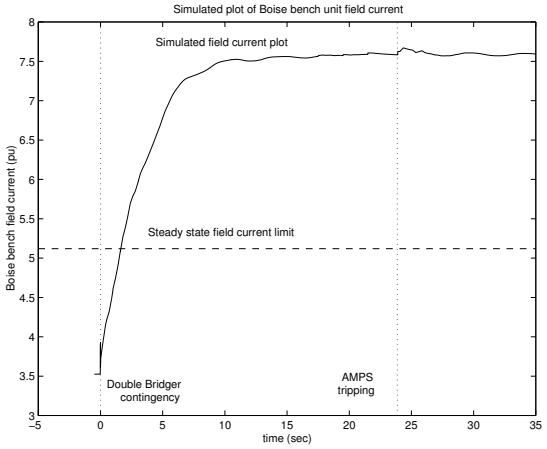

Figure 19. Boise bench field current

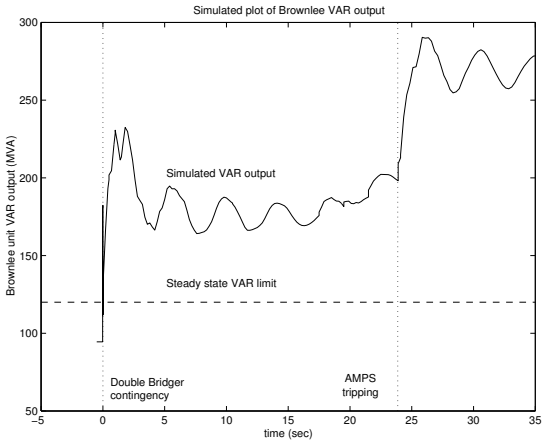

Figure 20. Brownlee field current

For a more accurate representation of the voltage behavior at low voltages, the loads in the Idaho area are partially represented (40%) by induction motors in the simulations. The load models for the rest of the system are retained the static load models in the base case stability data. The simulation of the Boise voltage with these modifications (limiters on Idaho units and 40% induction motor representation of Idaho loads) is shown in Figure 21.

The time-plots of field currents in the simulation in Figure 22 show that the field over-current limiters become activated both at Boise bench condenser and Brownlee generators and the Boise voltage collapses rapidly in the simulation after the limiters come into effect.

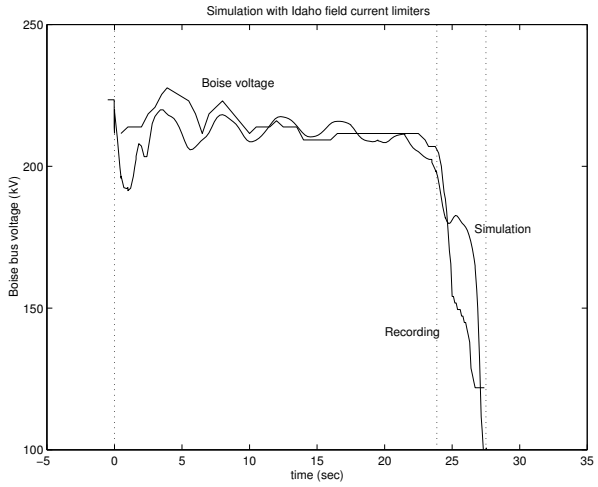

Figure 21. Simulation with Idaho field current limiters and induction motor loads

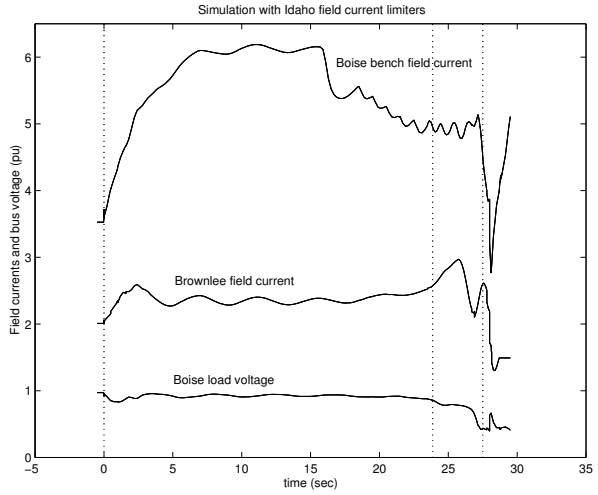

Figure 22. Effect of field current limiters

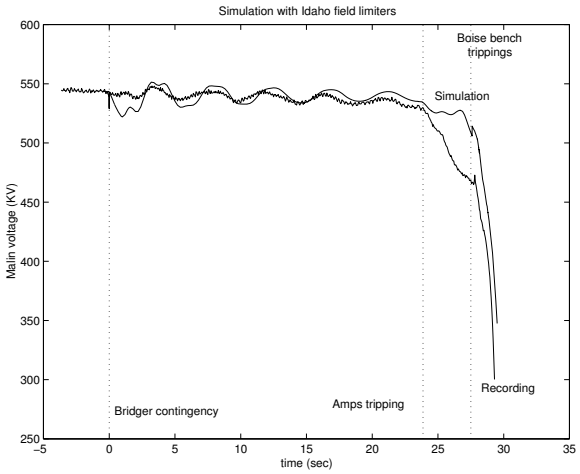

Figure 23. Malin bus voltage decline is slower

In the simulation however, the collapse of the Malin bus voltage (Figure 23) is slower than it was during the July 2nd event.

Excitation over-current limiters were also represented on the Northwest generators John Day, Dalles, and McNary in the simulation. These limiters become activated in the simulation during the fast collapse of the Malin voltage, which proceeded the tripping of the COI lines. Moreover, since the transient response of governors in thermal units would be quite slow when they operate near their ratings, governors on all thermal units with ratings above 100 MW were blocked in our 30-second simulation of the July 2nd disturbance. The simulated response of the COI power-flow matches better with the actual power-flow after the blocking of governors. Compared with the validated model of the August 10, 1996 model that is presented in Section 3, the duplication of the COI MW response in the July 2, 1996 model was more difficult. The model based simulation showed larger amplitudes of COI MW swings as compared to actual system recordings.

2.2.1.1 Model enhancements:

In summary, the following modifications were incorporated in the final validation model, which closely captures the actual behavior of the system response during the July 2nd event.

1) Excitation Over-current Limiters:

a) Excitation over-current limiters were modeled on units in the Idaho area. In the simulation, the limiters at the Boise Bench condenser and the Brownlee unit are activated right after the tripping of the Amps line which in turn induces the fast voltage collapse at Boise.

b) Excitation over-current limiters were represented at John Day, Dalles, and McNary units in the Northwest area. In the simulation, John Day and Dalles limiters are activated shortly after the Boise Bench line trippings, which accelerate the collapse of the COI bus voltages.

2) Nonlinear dynamic Load models:

a) Loads in Idaho were represented by 40% Induction motor loads (H=1 sec) and 60% Constant Current loads.

b) Boise load was tuned to match the recorded voltage response at the Boise load bus.

3) Blocking of governors:

Governors were blocked on all those thermal units in the WSCC system with ratings above 100 MW.

2.2.1.2 Time-domain simulations:

This subsection summarizes comparisons of actual time-recordings versus ETMSP simulations of the July 2nd disturbance. With the minor modifications of the stability data stated in Section 2.2.1.1, it is seen that the simulated responses closely match the time-recordings.

The simulations of the Malin (Figure 24), and Boise (Figure 25) bus voltages compare very well with the respective time-recordings as shown below. The amplitude of the Malin voltage oscillations in the simulation is somewhat higher in the initial 24 seconds of the event as compared to the recording, which may be related to possible deficiencies in exciter models of key Northwest generators supporting the COI lines. However, the overall behavior of the bus voltages is nicely captured in the simulations throughout the disturbance event including and up to the tripping of the COI lines.

The simulations of the Garrison bus voltage (Figure 26) and the COI MW power-flow (Figure 27) are shown next. While the simulated COI MW power-flow response follows roughly the behavior of the time-recording, the amplitude of the 0.225 Hz inter-area mode in the simulated response is more than the amplitude of the oscillations in the actual time-recordings. Also, the COI power-flow swings appear to be somewhat better damped in the simulated response as compared to the recorded response. These issues related to simulation of the COI MW flow need to be better understood in future studies.

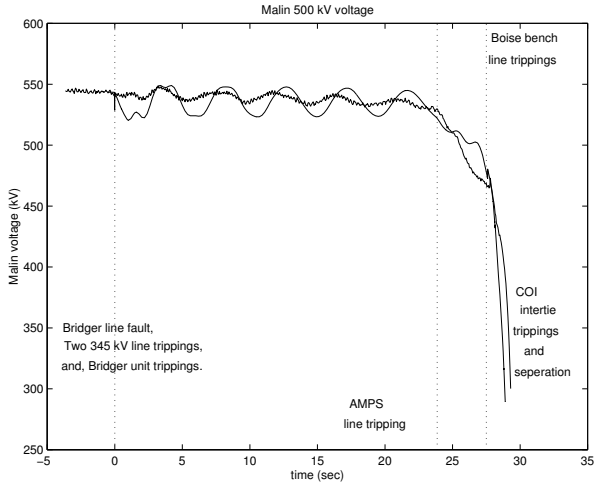

Figure 24. Malin voltage simulation for the validated model

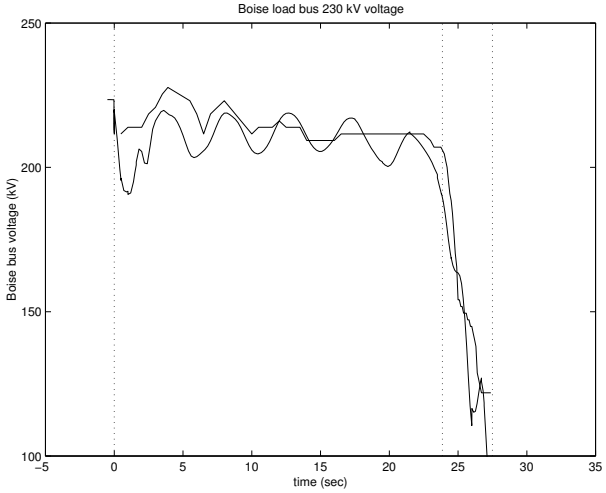

Figure 25. Boise voltage simulation for the validated model

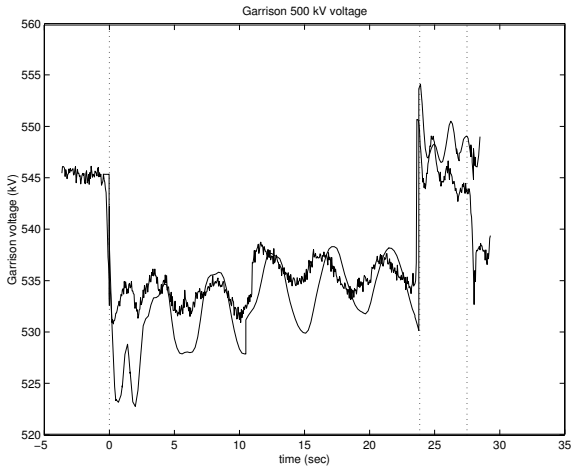

Figure 26. Garrison 500 kV voltage simulation for the validated model

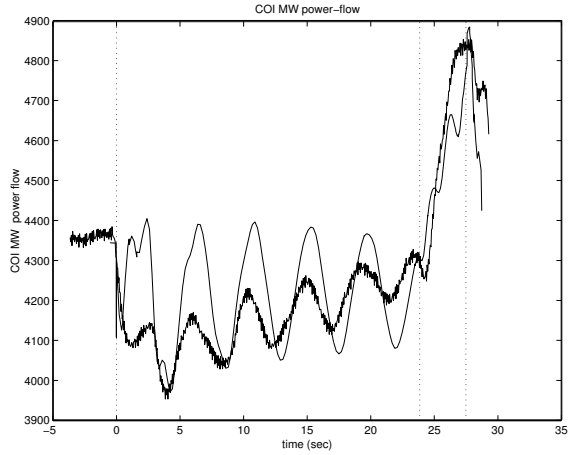

Figure 27. COI active power-flow simulation for the validated model

The simulated MVAR flow on COI lines (Figure 28) also roughly follows the recorded response, and the PDCI MW power-flow (Figure 29) compares well with the recording.

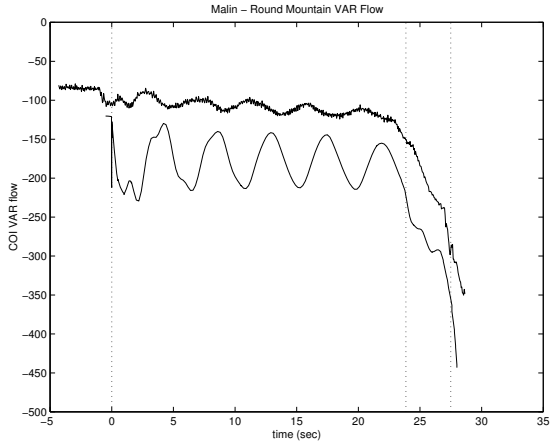

Figure 28. COI reactive power-flow simulation for the validated model

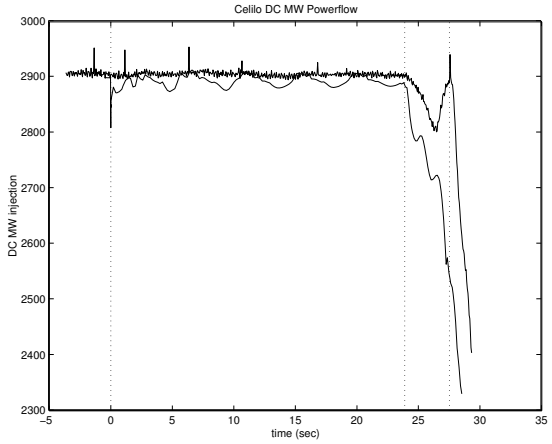

Figure 29. PDCI HVDC power-flow simulation for the validated model

The simulated San Francisco frequency (Figure 30) matches very well with the recorded San Francisco frequency. On the other hand, the Tacoma frequency response (Figure 31) is less closely duplicated in the simulation.

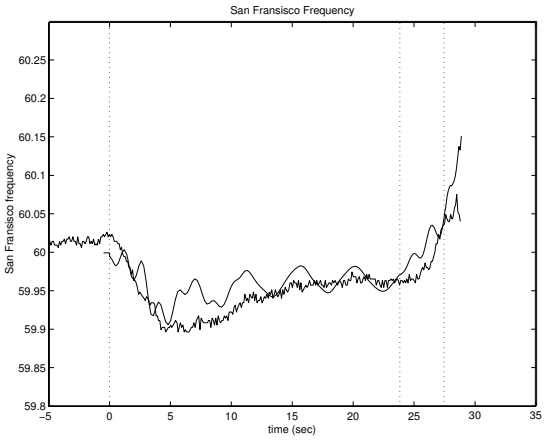

Figure 30. San Francisco load frequency simulation for the validated model

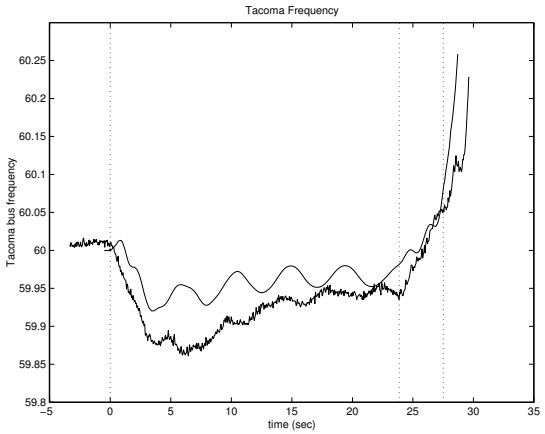

Figure 31. Tacoma frequency simulation

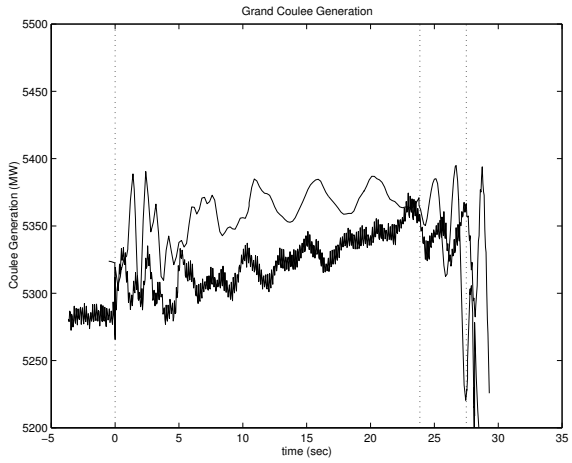

Figure 32. Grand Coulee generation for the validated model

Simulations of generations at Coulee (Figure 32) and McNary (Figure 33) are shown next.

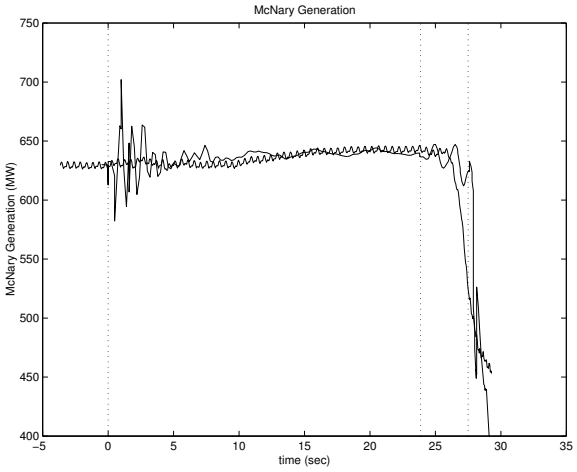

Figure 33. McNary generation for the validated model

In summary, the ETMSP simulations of the stability data with the modifications listed in Section 2.2.1.1 match very well with the actual time-recordings of the July 2nd disturbance event.

2.2.1.3 Singularity of the DAE equations:

Under quasi-stationary phasor assumptions [6], the dynamics of the power system can be modeled by a set of differential-algebraic equations of the form

$$\frac{dx}{dt} = f(x, y, p) \qquad (1)$$

$$0 = g(x, y, p) \qquad (2)$$

$$x \in R^n, y \in R^m, p \in R^q,$$

$$f : R^{n+m+q} \to R^n, \; g : R^{n+m+q} \to R^m$$

Here the *f* equations (1) denote the dynamics of the generators, control devices and loads. Whereas the *g* equations represent the power balance equations of the transmission network under the quasi-stationary assumption. The state variables *x* correspond to the internal dynamic state variables of the dynamic devices. The algebraic *y* variables represent the power-flow variables, namely, the bus voltage magnitudes and bus voltage angles. The system and operating parameters are denoted *p*. When the *x* variables change as dictated by their dynamics, the *y* variables will also change instantaneously so as to satisfy the network constraints (2). This is well known as the differential-algebraic formulation of the power system midterm dynamic models. Naturally, the power system simulation programs such as ETMSP also have built-in algorithms for handling the special constrained nature (1)-(2) of the power system models [14].

The constrained formulation (1)-(2) becomes problematic when the dynamics approaches the singularity *S* of the constraint equations (2) defined as

$$S = \left\{ (x, y, p) : g(x, y, p) = 0, \det\left(\frac{\partial g}{\partial y}\right)(x, y, p) = 0 \right\} \quad (3)$$

For the constrained model, the algebraic variables *y* normally change according to

$$\frac{dy}{dt} = -\left(\frac{\partial g}{\partial y}\right)^{-1}\left(\frac{\partial g}{\partial x}\right) f(x, y, p) \qquad (4)$$

so that the *y* dynamics satisfies the network constraints (2). Clearly, near the singular points in *S*, the speeds of some of the *y* variables, namely, some bus voltage magnitudes and bus voltage phases can become large because of the inverse of the singular Jacobian in (4). The role and implications of the singular points *S* have been discussed extensively in power system literature. In our previous publication [6], we had noted that the underlying quasi-stationary assumption in formulating the model (1)-(2) may be violated near the singularity *S*, and hence, the results of the model (1)-(2) need to be treated with caution near the singular points.

In power system computational programs such as ETMSP, the network equations (2) are normally solved to update *y* in each iteration step after updating a new value for the dynamic variables *x*. In this context, the computational programs also have a difficult time near singular points because the network equations become stiff. The Newton-Raphson algorithm that is typically used for solving the algebraic equations (2) displays convergence problems when the network Jacobian $\frac{\partial g}{\partial y}$ is close to singular, as is the case near the singular points in *S*.

In carrying out the model validation of the July 2, 1996 western system, the simulation program encountered singular points just after the tripping of the Amps line. The program ETMSP abruptly ended with the message that the network equations were too stiff to proceed. This was prior to the collapse of the Boise load voltage in the simulation in Figure 18. In order to improve convergence of the network equations,

the number of iterations for the algebraic network solution was increased, and the step size for numerical integration was decreased to 1 millisecond. This is in sharp contrast to typical step sizes of 8 milliseconds, which are normally used in large scale simulations. With the modifications, the ETMSP simulation closely followed the sharp voltage collapse at Boise in the actual Boise bus voltage recording. The stiffness of the power-flow equations in ETMSP during the simulation of the fast Boise voltage collapse indicates the proximity of the system model to the power system singularity *S* of the network equations.

Note that the Boise bus voltage is a power-flow variable, part of the *y* variables in the model (1)-(2), in the ETMSP model. The fast decline from about 210 kV to 150 kV in about three seconds (from the actual recording) is also consistent with the theoretical expectation that some of the algebraic variables such as key bus voltages will change fast near the singular points. Therefore, *the simulations and actual recordings both confirm that the response of the western power system was influenced by the power system network singularity S just after the tripping of the Amps line.* The singularity resulted in fast voltage collapse at Boise. The speed of the collapse was significant in that it prevented any possible operator intervention before the lights went out at Boise.

Voltages near 150 kV correspond to fault-on like values for voltages and currents in the Idaho area. Since the collapsed area was not completely isolated, the reactive power surged into the Idaho area over the next few seconds over all the lines connected to the Idaho area, and the surges in currents and reactive power (as well as real power) meant that the low voltage conditions spread quickly in all directions that remained electrically connected to the Idaho region. Within a few seconds after the Amps line tripping and after the Boise voltage collapse, the voltages on COI tie-lines also collapsed down to 300 kV on the 500 kV buses that led to the tripping of the COI lines and to system separation.

In later simulations, we will see that the voltage collapse might have been much slower if some of the susequent line and generation trippings had not occurred. The slow voltage collapse, which has been experienced earlier in power systems, was made more and more severe by the line trippings as they occurred, and eventually, the power system was pushed into the proximity of the power-flow singularity that led to the fast voltage collapse.

The recordings and the simulations of the July 2, 1996 event clearly establish that power system singularity can occur in real systems and it can be extremely harmful to system operation. The authors also believe that the singularity likely played a role in the recent August 14, 2003 northeastern blackout. *We conjecture that the fast voltage collapse in the Cleveland area and the fast real power swings that were experienced over the next few seconds were likely caused by the system dynamics entering into the singular domain S of the power-flow equations.*

The implications of the singularity for future power system operations and contingency conditions need to be carefully looked into.

2.2.2. Sensitivity studies of the switching sequence:

In this section, sensitivity studies are carried out using ETMSP based simulations of the validated stability case of the previous section.

The first set of sensitivities is aimed at studying the effect of each of the switching events, which occurred during the July 2nd disturbance. First, we start with the line fault on the Bridger to Kinport 345 kV line and the clearing of this fault.

2.2.2.1 Normal fault-clearing of Bridger to Kinport 345 kV line-fault:

The system recovers nicely to its operating condition after the line-fault on the Bridger to Kinport 345 kV line is cleared normally by opening of this line. Note that both Malin and Boise voltages settle to near one per unit values, and the 0.25 Hz COI inter-area mode oscillations are well damped.

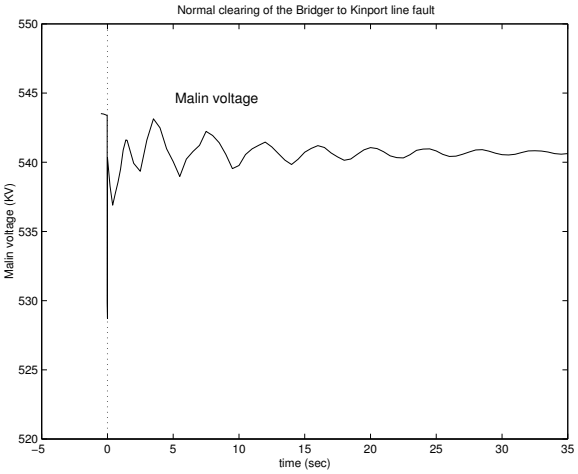

Figure 34. Malin voltage after the first line outage

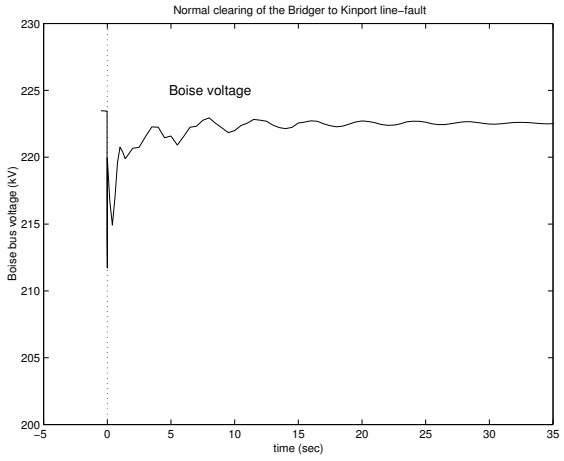

Figure 35.Boise voltage after the first line outage

2.2.2.2 Two Bridger line outage contingency:

After the line-fault on the Bridger to Kinport 345 kV line, because of faulty relay operation, the parallel 345 kV line from Bridger to Goshen was also tripped during the July 2nd event. The remedial action scheme (RAS) for this double contingency includes 1) tripping of two 550 MW Bridger generator units, 2) series capacitor by-pass on Bridger to Borah 345 kV line and Summer Lake to Burns 500 kV line, and, 3) switching of 175 MVAR shunt capacitor bank at Kinport bus. The next simulation of this double contingency with the RAS scheme shows that the transient would have recovered after this contingency, even though the Boise voltage settles to a low voltage value 205 kV after the contingency.

Previously in power-flow analysis, it was shown that the Idaho system was reactive power deficient after the double Bridger contingency with a negative margin of –140 MVAR at Boise after the tripping of the two Bridger lines and its associated RAS scheme. However, the transient simulation of the contingency here with the validation model shows a transient recovery for simulation up to 100 seconds. During this transient, the field over-current limiters at Boise bench synchronous condenser and Brownlee become activated at about 15 seconds and 30 seconds after the initiating event respectively, and the Boise voltage decreases to the lower value 205 kV. As stated in Section 1.1, the loads in the validation model consist of a) voltage dependent static composite loads (a mixture of constant power, constant current, and constant power), and b) induction motor loads. Unlike the power-flow study that assumed constant MVA loads, the reactive demands of the loads change with the lower voltages in this transient study, and the system response does recover with no additional field current limiter actions in the simulation.

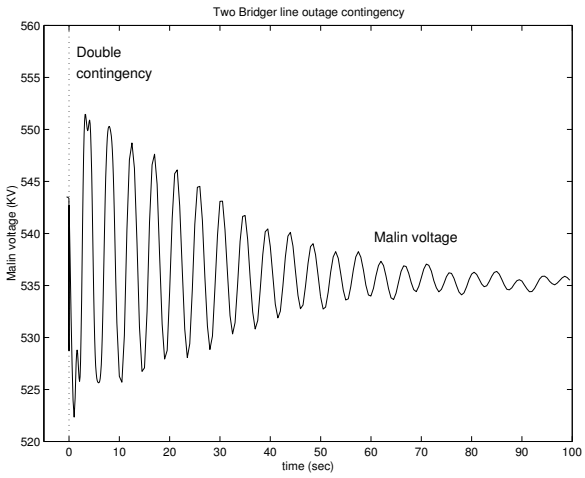

Figure 36. Malin voltage after the double Bridger outage

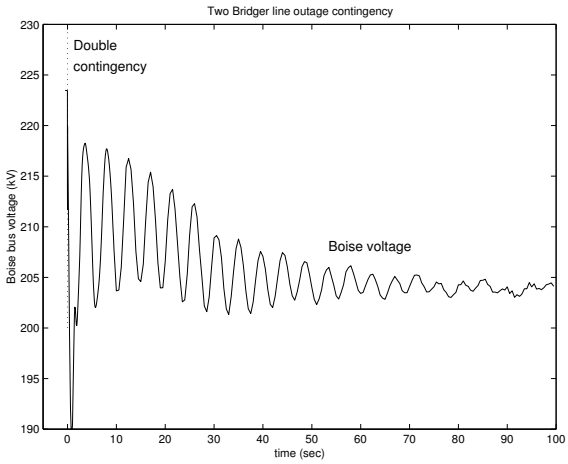

Figure 37. Boise voltage after the double Bridger outage

2.2.2.3 La Grande to Round-Up 230 kV line tripping:

The next switching event during the disturbance was the tripping of the La Grande to Round-Up 230 kV line about three seconds after the initial line-fault. The simulation of the contingency after the La Grande line tripping shows that Malin and Boise voltages are slightly lower with the loss of the 230 kV line. Again, the transient recovers after the line tripping in the simulation. Therefore, the tripping of the La Grande to Round-Up line may not have been a significant switching event during the July 2nd disturbance. This is also consistent with the power-flow study where the VAR deficiency did not change much after the La Grande line tripping.

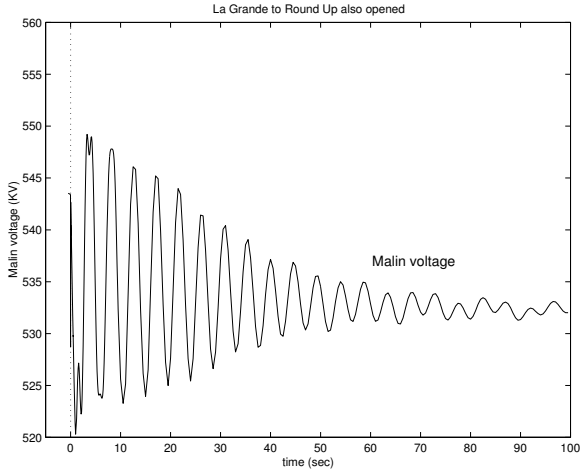

Figure 38. Malin voltage after the La Grande line trip

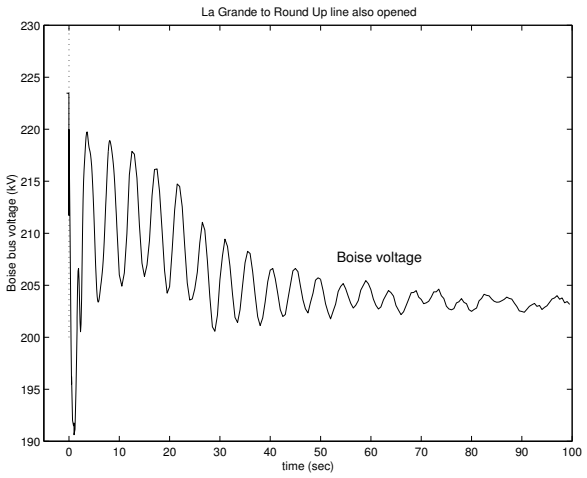

Figure 39. Boise voltage after the La Grande line trip

2.2.2.4 Anaconda capacitor bank switching:

Next, when the 59 MVAR capacitor bank is switched in at Anaconda, the transient shows little change in Malin and Boise voltages in the simulation. Note that this is consistent with the power-flow analysis, which showed that the reactive power deficiency in the Idaho area did not change much with the switching of the Anaconda capacitor bank.

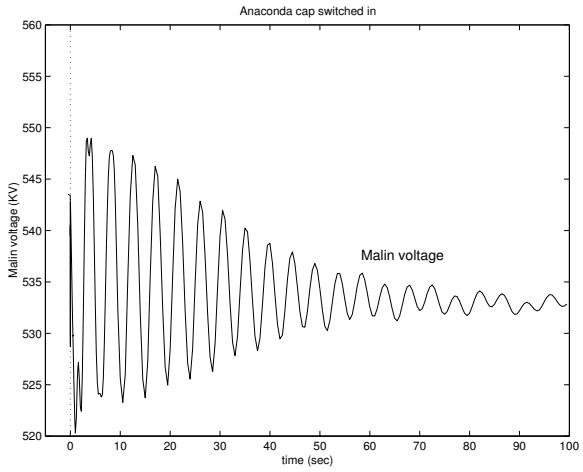

Figure 40. Malin voltage after Anaconda cap insertion

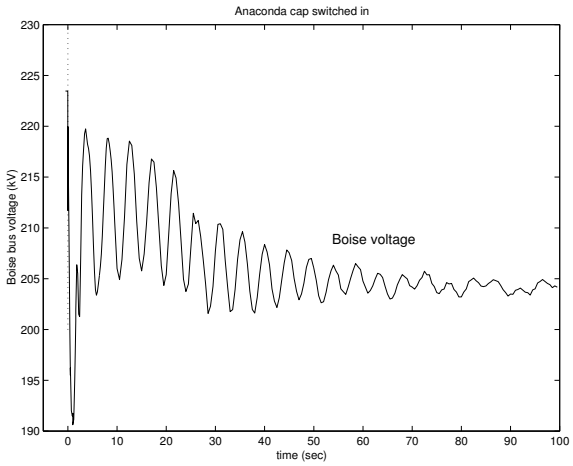

Figure 41. Boise voltage after the Anaconda cap insertion

2.2.2.5 Tripping of Strike generator units:

Three generator units at Strike plant with a total generation of 80 MW were tripped during the event because of over-excitation related protective relay action. In the first simulation (Figures 42 and 43), two of the Strike units with 27 MW generation each are tripped next at 18 and 21 seconds after the initial fault clearing.

When all three Strike units are tripped, there is no longer a stable equilibrium for the resulting system, and a slow voltage collapse results in the simulation. Previously, in the power-flow studies, we observed that the reactive power deficiency in the Idaho area becomes much larger with the dropping of the Strike units. In this transient simulation, field over-current limiters become activated at several Idaho generators sequentially, and the Boise voltage collapses slowly in a classic voltage collapse like scenario. Modeling of slow voltage controls such as tap changers and shunt capacitor banks may be necessary for simulating the scenario properly.

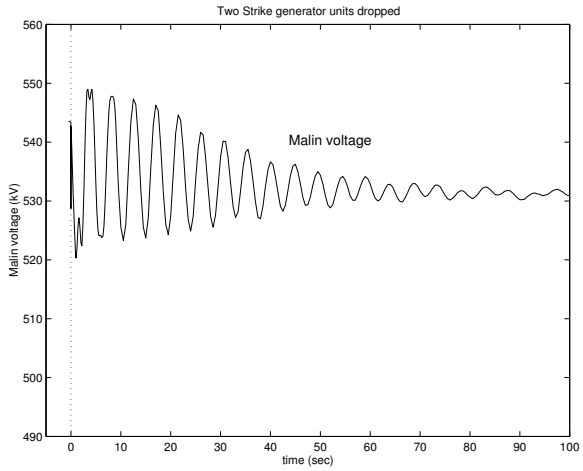

Figure 42. Malin voltage after tripping of two Strike units

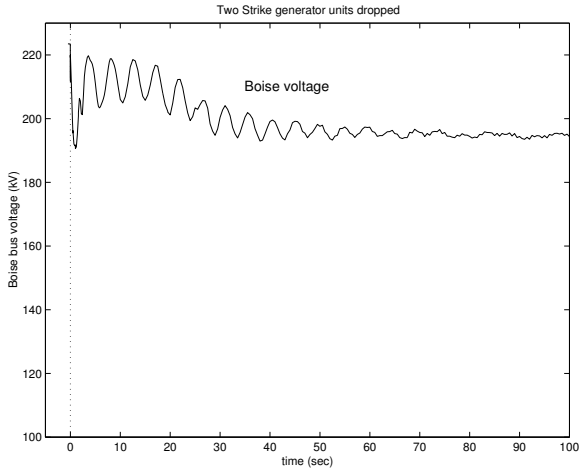

Figure 43. Boise voltage after tripping of two Strike units

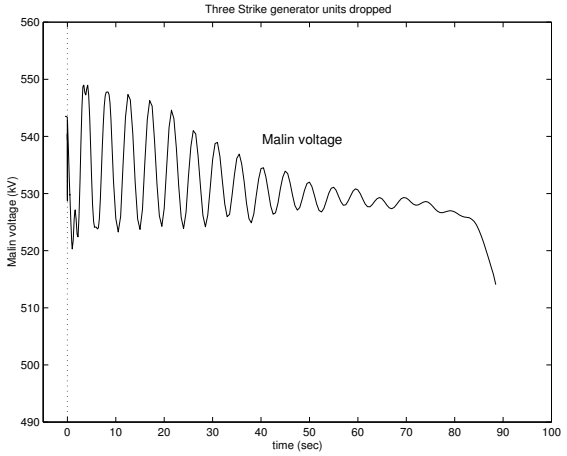

Figure 44. Malin voltage after tripping of three Strike units

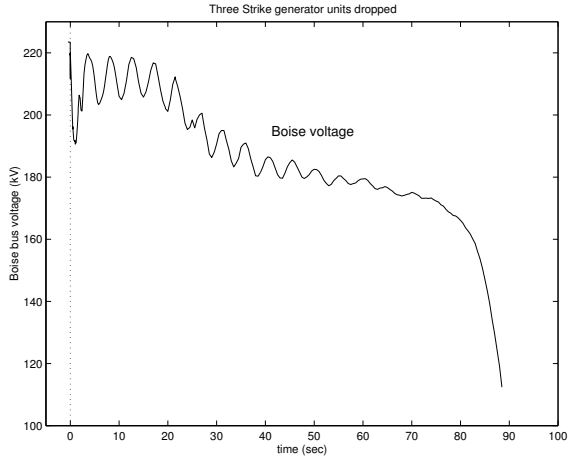

Figure 45. Boise voltage after tripping of three Strike units

In other words, in the absence of additional tripping events, the system might have undergone a slow voltage collapse after the tripping of Strike units. In the next subsections, we will see that the voltage collapse becomes faster in the simulation with additional trippings as they occurred during the July 2nd disturbance. The fast nature of the collapse was significant in that the fast collapse prevented any possible operator intervention during the event.

Dynamically, we postulate that the power system underwent a saddle node bifurcation in the simulation with the tripping of the three Strike units. A saddle node bifurcation occurs when a stable equilibrium point collides with an unstable equilibrium point under parametric variations, and the two annihilate each other. Saddle node bifurcations are usually associated with the presence of a zero real eigenvalue in the system Jacobian. Previously in Section 2.1, in power-flow analysis, we had shown that the system operation was pushed outside the power-flow feasibility region outside the static bifurcation boundary by the tripping events during the July 2, 1996 event. Roughly speaking, since the power-flow equations normally correspond to the steady state equilibrium solutions of the power system dynamic model (1)-(2), the static bifurcations of the power-flow equations roughly correspond to the dynamic saddle node bifurcations in the full dynamic model (1)-(2). However, owing to differences in the load models and generator exciter representation etc., the power-flow static boundaries are typically more conservative than the dynamic saddle node bifurcation boundaries.

In Section 2.1, the system was pushed outside the static bifurcation boundary in Case C itself, that is, right after the double Jim Bridger outage. However, in dynamic simulations, the operation is rendered outside the saddle node bifurcation boundary after the tripping of the three Strike units (that corresponds to Case F in Section 2.1). With the disappearance of the stable equilibrium point, a slow diverging transient results along the center manifold direction of the remnants of the equilibrium [15]. *The slow decline is a signature of the occurrence of the saddle node bifurcation phenomenon in dynamic models.*

Also, when the operation moves outside the saddle node bifurcation boundary, the transient would be slower or faster depending on how close or far the parameter values are to the saddle node boundary respectively. We illustrate this fact in the next simulation plot. In Figure 46, the simulation of Figure 45 is repeated after switching in variable amounts of shunt capacitor banks at Boise Bench at 3 seconds after the tripping of the Strike units. In Figure 45, the Boise voltage collapsed at about 87 seconds after the initial fault clearing. With the switching in of shunt compensation at Boise, the parameter values move closer towards the saddle node bifurcation boundary. Accordingly, the Boise collapse becomes slower in the simulations in Figure 46.

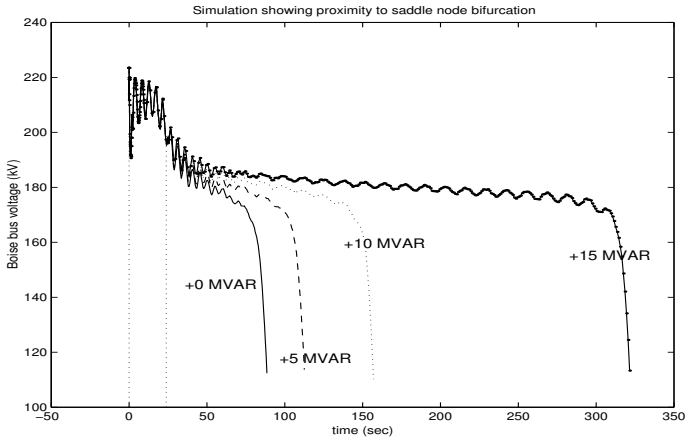

Figure 46. Effect of saddle node bifurcation boundary on the Boise voltage collapse

When there is no additional shunt compensation, the collapse is at about 87 seconds (solid plot in Figure 46) after the initial fault event. When +5 MVAR is switched in at Boise, the Boise collapse slows down to at about 113 seconds (dashed plot in Figure 46) after the initial event. After +10 MVAR is switched in at Boise, the collapse is even slower at about 157 seconds (dotted plot in Figure 46) after the initial fault. When +15 MVAR is switched in, the collapse is very slow at about 322 seconds (bold dotted plot in Figure 46) after the first fault event. These simulations support our hypothesis that the *system underwent a saddle node bifurcation with the tripping of the Strike units.* As such, it is very difficult to compute the presence of zero real eigenvalue in large scale power system models owing to excessive computational burden. Future research is encouraged at developing techniques for locating the saddle node bifurcation boundaries in dynamic large scale models of the form (1)-(2).

2.2.2.6 Tripping of Lucky Peak generator:

At 23 seconds after the initial fault, the Lucky Peak generator is tripped next. The Boise voltage now collapses within 12 seconds after the tripping of the Lucky Peak generator in Figure 48.

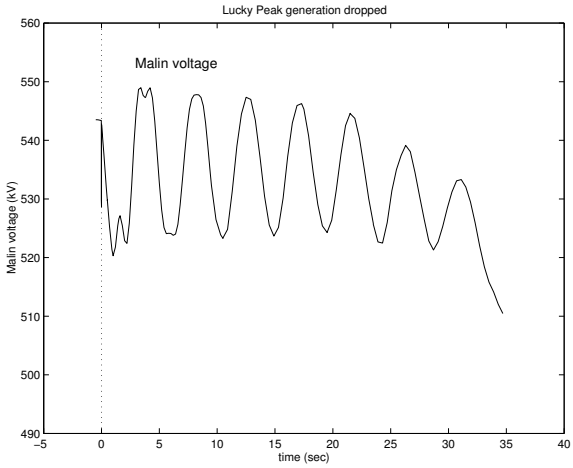

Figure 47. Malin voltage after the tripping of Lucky Peak generator

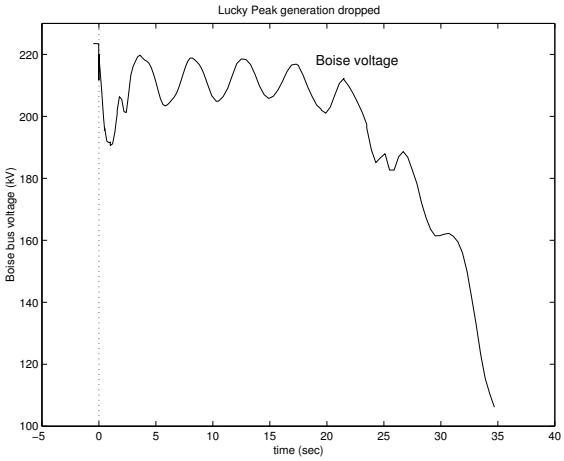

Figure 48. Boise voltage after the tripping of Lucky Peak generator

2.2.2.7 Tripping of Antelope to Anaconda 230 kV line:

The 230 kV line from Antelope to Anaconda (Amps line) was tripped during the July 2, 1996 disturbance because of a Zone 3 relay tripping. Boise voltage collapsed from about 200 kV to about 120 kV within three seconds after the Amps line tripping during the disturbance. The next simulation (Figures 49 and 50) of the system response with the switching sequence up to and including the Amps line tripping agrees well with the actual Boise voltage recording from the disturbance.

2.2.2.8 Events up to the tripping of COI lines:

In Section 1.2, it was shown that the simulation of the transient matches very well with actual recordings up to the tripping of COI lines was presented. Again, note that the speed of voltage decline at Boise prevented any possible operator intervention during the disturbance. The simulations in this section have showed that the collapse itself resulted from a "slow" transient after the loss of a viable stable equilibrium point. Specifically, the tripping of Strike generator units moved the system across the saddle node bifurcation boundary in our simulation. The later switching events namely the tripping of Lucky Peak generator and Amps line tripping pushed the system further away from recovery, and along a fast diverging transient.

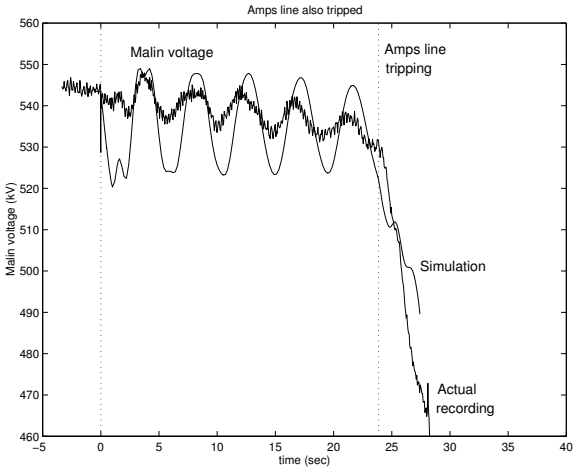

Figure 49. Malin voltage after the Amps line tripping

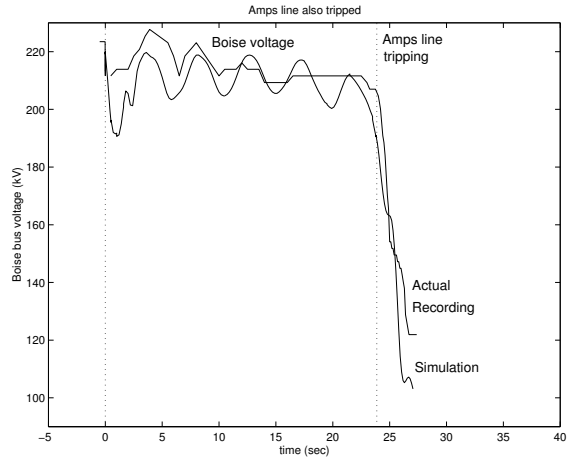

Figure 50. Boise voltage after the Amps line trip

2.3. Sensitivity studies of potential control actions:

In this section, we study the impact of potential control actions that could have been implemented during the July 2, 1996 event.

2.3.1 Sensitivity study of 0.25 Hz inter-area mode damping:

During the 22 seconds time-period between the initiating event and the Amps line tripping, poorly damped 0.22 Hz inter-area mode oscillations were also present during the July 2nd disturbance. In this simulation, load models in the Northwest, Idaho, and British Columbia areas were adjusted to improve the damping of the 0.22 Hz mode in the simulation. The switching sequence in the simulation matches that of the disturbance, and is the same as for the validation studies of Section 1. In the simulation, Boise voltage collapses after the Amps line tripping, as was the case during the event. After the tripping of Boise bench lines, the COI bus voltages collapse as well in the simulation. This simulation establishes that the poorly damped nature of the 0.25 Hz mode did not affect the nature of voltage declines during the July 2nd disturbance event. The July 2nd event was mainly a voltage instability phenomenon, whereas the August 10th WSCC disturbance was a small-signal instability phenomenon [2]. We will discuss the August 10, 1996 event in detail in Section 3.

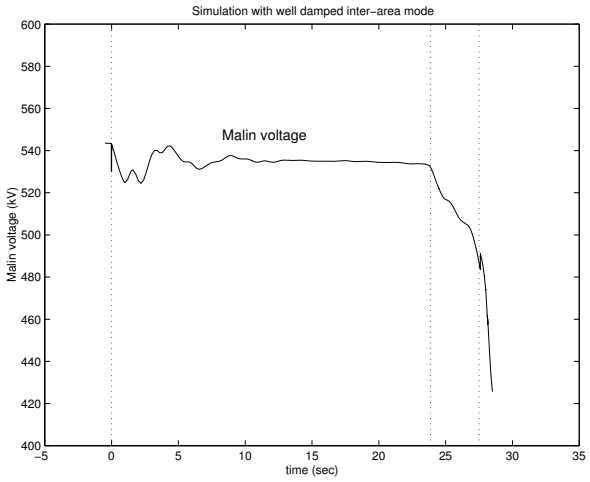

Figure 51. Malin voltage for well-damped case

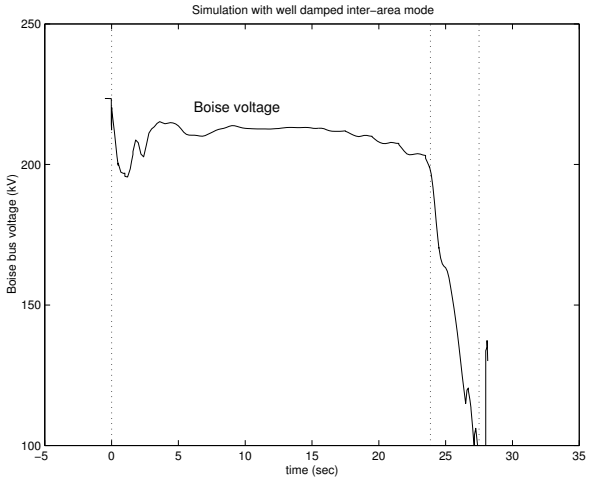

Figure 52. Boise voltage for the well-damped case

2.2.3.2 Sensitivity to Malin capacitor banks:

During the July 2nd event, the Malin shunt capacitor banks did not switch in during the initial 24 seconds prior to AMPS line tripping owing to the presence of poorly damped 0.22 Hz mode oscillations of the Malin 500 kV voltage. In power-flow studies in Section 2.1.3, we showed that the switching of capacitor banks at Malin would not have helped the reactive power problems in the Boise area. We revisit the same question using time-domain simulations.

In this simulation, the time-delays of the switching logic are assumed to be faster so that one 200 MVAR bank switches in at 6.5 seconds after the initiating fault sequence. Another 200 MVAR bank switches in at 25.5 seconds into the event, which is one second after the AMPS line tripping. In the simulation, the switching sequence matches the July 2nd switching sequence

up to and including the Amps line tripping. The Boise voltage collapses in this case as well (Figure 54) after the Amps line tripping. The simulation shows that switching of Malin capacitor banks does not affect much the reactive power deficiency in the Boise area, and this observation is also consistent with the power-flow sensitivity studies. The collapse at Malin would have been somewhat slower by about 5 seconds (Figure 53) with the earlier switching of Malin cap banks.

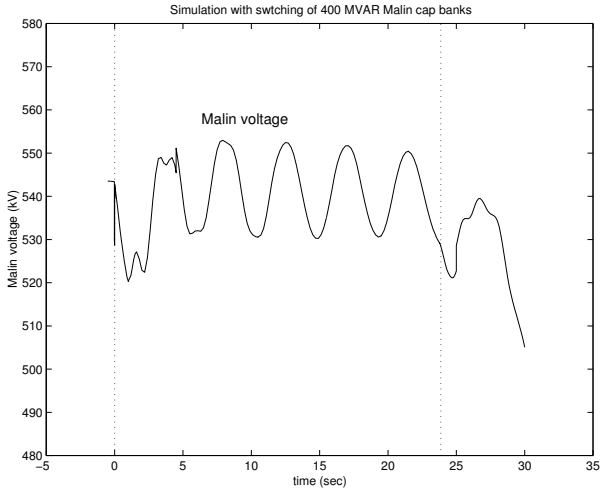

Figure 53. Malin voltage with faster insertion of Malin cap banks

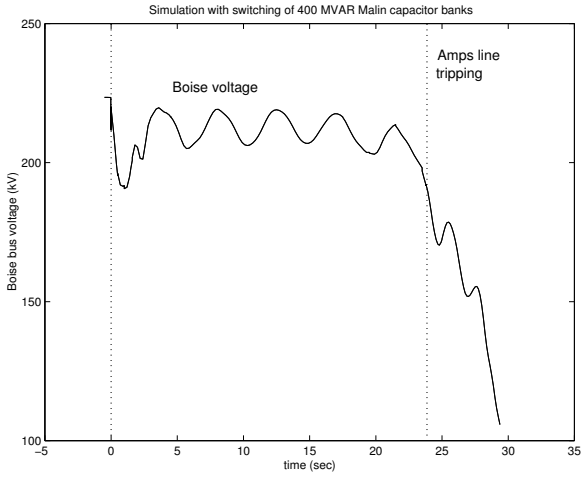

Figure 54. Boise voltage with faster insertion of Malin cap banks

2.2.3.3 Sensitivity to Series capacitor by-pass:

In the power-flow study, it was shown that the reactive deficiency in the Idaho area after the Bridger two line outage contingency was partially caused by by-passing of the series capacitors on Bridger to Borah 345 kV line and Summer Lake to Burns 500 kV line. In this simulation, the same sequence of July 2nd event is carried out excepting that the series capacitor by-pass after the Bridger contingency is blocked.

With the series capacitor banks in service, the Boise area voltages are at near normal voltages close to 1 per unit after the initial double contingency and the field currents of the Idaho units also are below their steady state limits. If the field current limiters did not interfere, the voltages in the Idaho area may not have collapsed. However, if we assume that the sequence of trippings progressed as it did during the event with the same timings, then the Boise voltage collapses (Figure 56) after the Amps line tripping. As compared to when the capacitor banks are by-passed, the Boise voltage decline is slower with the series capacitors in service.

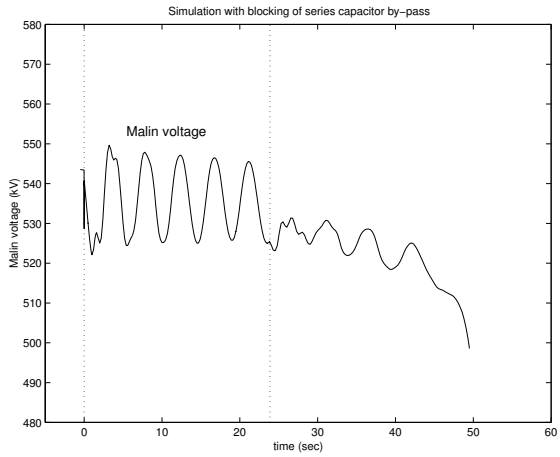

Figure 55. Malin voltage with blocking of series cap bypass

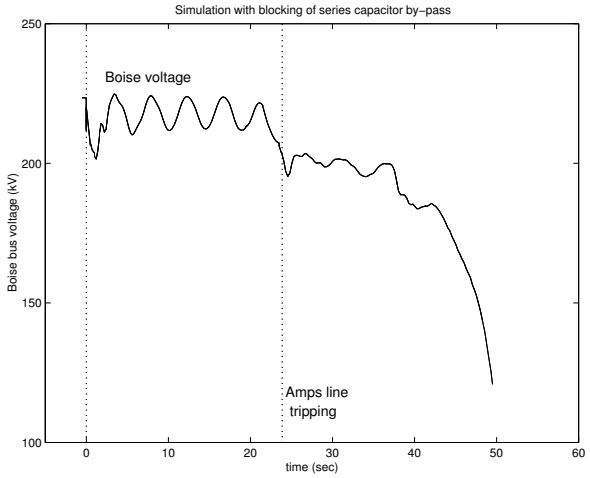

Figure 56. Boise voltage with blocking of series cap bypass

2.2.3.4 Sensitivity to Capacitor banks at Boise and Brownlee:

2.2.3.4.1 Switching of 100 MVAR at Boise and 100 MVAR at Brownlee:

In power-flow studies, it was shown that an additional shunt compensation of at least 175 MVAR each is necessary at Boise and Brownlee buses to get a valid power-flow solution for Case H power-flow after the tripping of Amps line. In this simulation (Figures 57 and 58), additional capacitive support of 100 MVAR each at Boise and Brownlee buses is switched

in. The simulation shows that the Boise voltage collapses after the Amps line tripping, even though the Boise voltage decline is slower in this simulation than the collapse during the event.

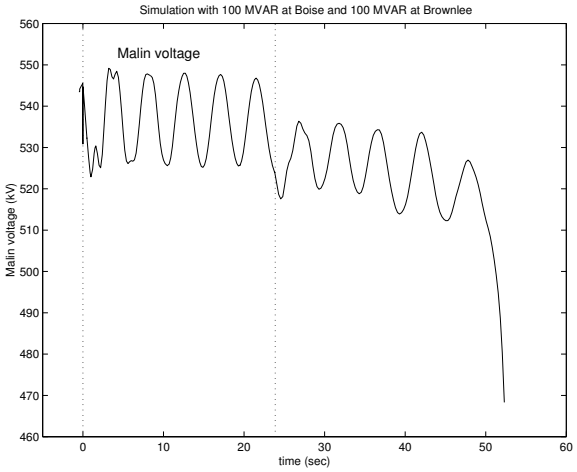

Figure 57. Malin voltage with +100 MVAR each at Boise and Brownlee

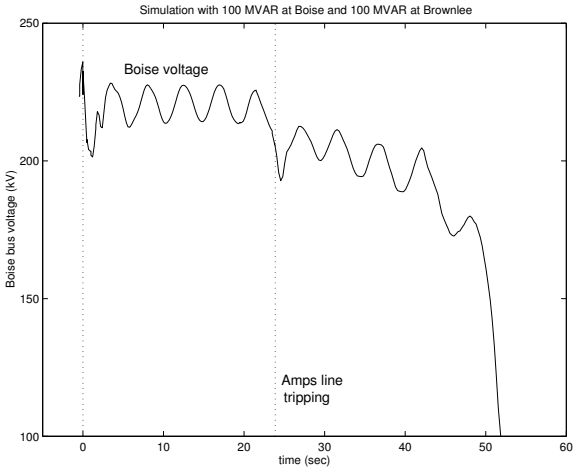

Figure 58. Boise voltage with +100 MVAR each at Boise and Brownlee

2.2.3.4.2 Switching of 150 MVAR at Boise and 150 MVAR at Brownlee:

In this simulation (Figures 59 and 60), two additional capacitor banks each rated 150 MVAR are assumed to be present at Boise and Brownlee 230 kV buses. With the additional VAR support, the system recovers to possibly acceptable operating condition even after Amps line tripping. The Boise voltage settles to a low voltage value about 200 kV in Figure 60.

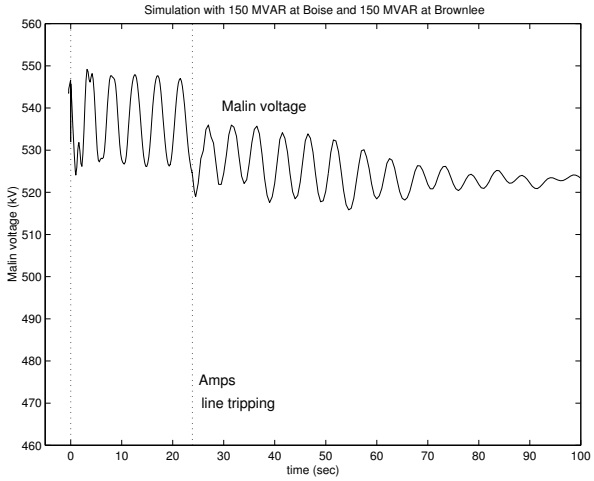

Figure 59. Malin voltage with +150 MVAR each at Boise and Brownlee

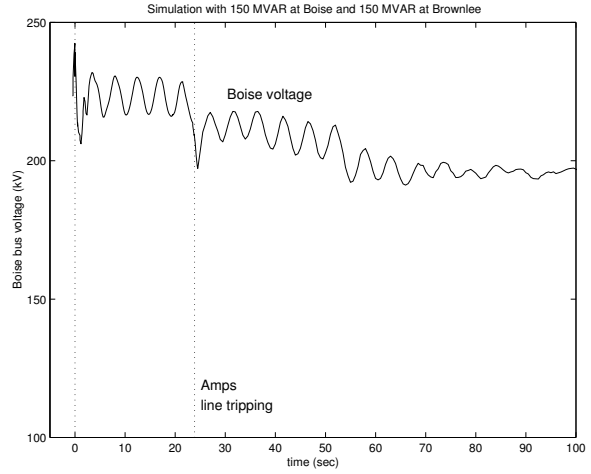

Figure 60. Boise voltage with +150 MVAR each at Boise and Brownlee

2.2.3.4.3 Switching of 200 MVAR at Boise and 200 MVAR at Brownlee:

With 200 MVAR capacitor support at each of Boise and Brownlee buses, the Boise voltage recovers to a higher voltage of 215 kV and the Malin voltage recovers to 525 kV. However, the presence of 0.25 Hz growing oscillations indicates that the 0.25 Hz COI inter-area mode may have become small-signal unstable after the Amps line tripping. The small-signal unstable oscillations are possibly even more troublesome for system operation as evidenced by massive system break-up resulting from the August 10, 1996 WSCC small-signal instability event. The damping properties of this mode need to be carefully analyzed for future control actions.

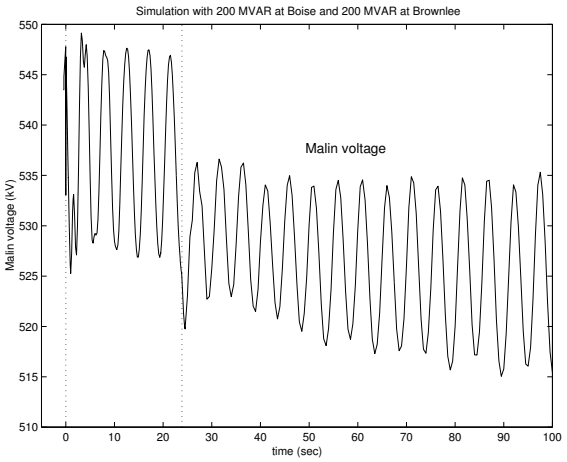

Figure 61. Malin voltage with +200 MVAR each at Boise and Brownlee

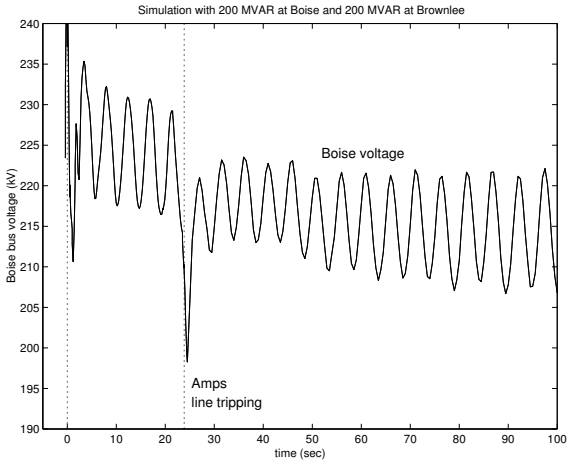

Figure 62. Boise voltage with +200 MVAR each at Boise and Brownlee

Recall that the power-flow studies showed earlier that shunt compensation of 200 MVAR each at Boise and Brownlee buses result in a valid power-flow solution after the Amps line tripping. However, *the presence of the oscillations in the transient study in this subsection with such shunt compensation points to the significance of studying potential control actions by transient analysis tools as well as small-signal analysis tools.*

2.2.3.5 Sensitivity to under-voltage load shedding at Boise:

The sensitivity studies of automatic undervoltage load shedding schemes in this subsection show that the load shedding schemes at Boise potentially could have been very helpful in mitigating the reactive power problems in the Boise area. However, the effectiveness of the schemes and the consequences are sensitive to the settings used in the load shedding schemes. Further research is indicated on developing a theory for proper setting of voltage thresholds and delay settings for the undervoltage load shedding schemes.

2.2.3.5.1 10% of Boise load shed at 0.9 per unit with a 2 seconds delay:

In the simulation, relays are programmed to shed 10% of the Boise when the Boise voltage stays below 0.9 per unit for 2 seconds. Then, the relays shed the 10% load 3 seconds after the initial fault. With the reduced load at Boise, the system appears to recover after Amps line tripping, even though the Idaho area voltage are somewhat low. Low voltages in Figures 63 and 64 also imply high line currents and further tripping of heavily loaded transmission lines is a possibility.

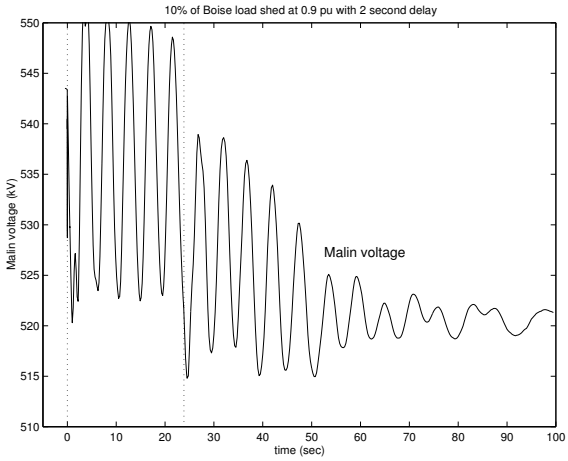

Figure 63. Malin voltage with load shedding at Boise

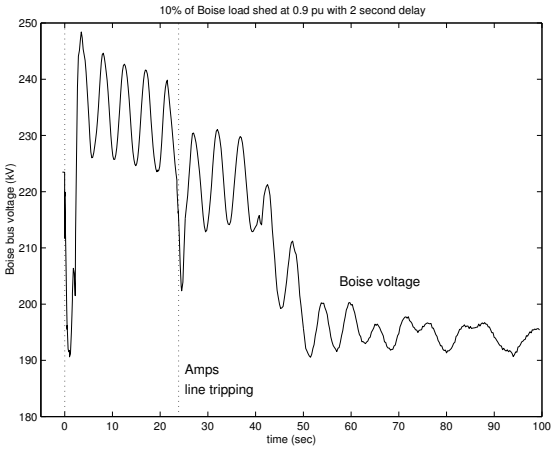

Figure 64. Boise voltage with load shedding at Boise

2.2.3.5.2 10% shed at 0.9 p.u. with a 2 seconds delay and 10% shed at 0.9 p.u. with a 5 seconds delay:

In this case, 10% of Boise load is shed at 3 seconds into the event, and an additional 10% is shed at 54 seconds into the event, and the Boise voltage recovers to a high value of about 245 kV.

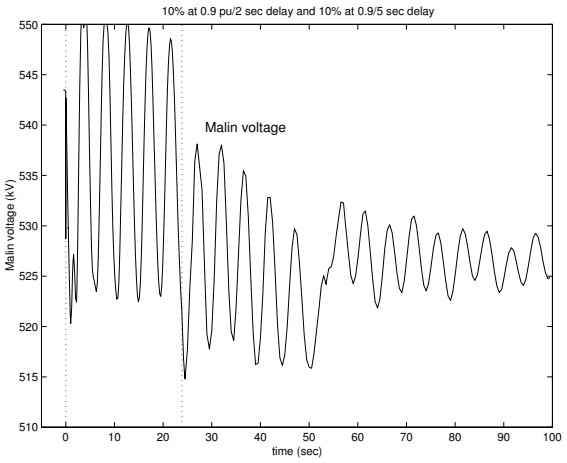

Figure 65. Malin voltage with load shedding at Boise

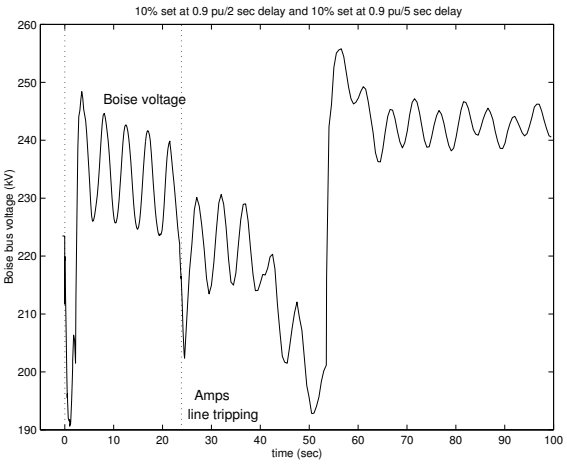

Figure 66. Boise voltage with load shedding at Boise

2.2.3.5.3 10% shed at 0.95 p.u. with a 10 seconds delay and 10% shed at 0.9 p.u. with a 10 seconds delay:

With these settings for the load shedding relays, 10% of the load is shed by the relay set for 0.95 per unit at 18 seconds into the event, and the other 10% is shed at 48 seconds into the event. The Boise voltage in Figure 68 again recovers to a high voltage 245 kV after the shedding of 20% Boise load.

2.2.3.5.3 10% shed at 0.9 p.u. with a 5 seconds delay and 10% shed at 0.85 p.u. with a 5 seconds delay:

When the relay settings are at 0.9 per unit with a 5 seconds delay, the relay sheds the load at 27 seconds into the event, which is at three seconds after the Amps line tripping (Figures 69 and 70). The Boise voltage has collapsed to 110 kV by that time in the simulation, and the load shedding of 10% Boise load does not result in voltage recovery.

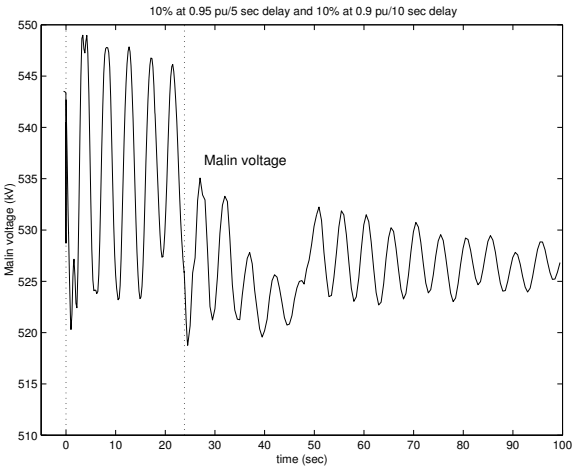

Figure 67. Malin voltage with Boise load shedding

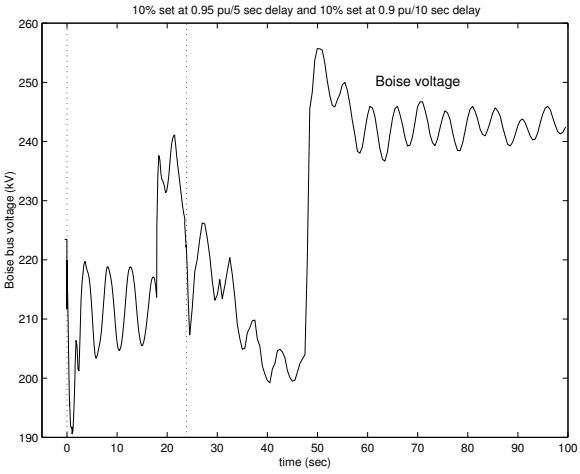

Figure 68. Boise voltage with Boise load shedding

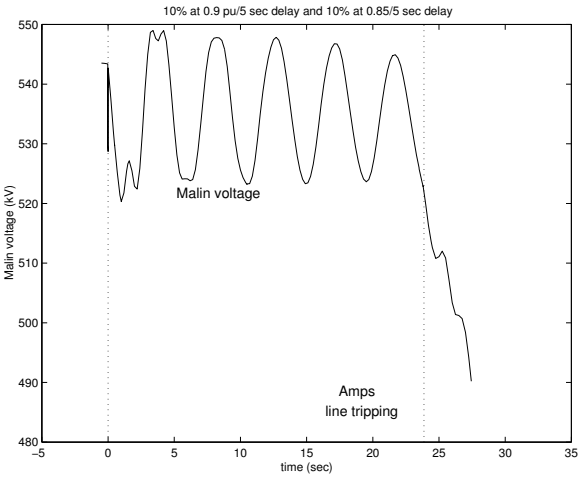

Figure 69. Malin voltage with Boise load shedding

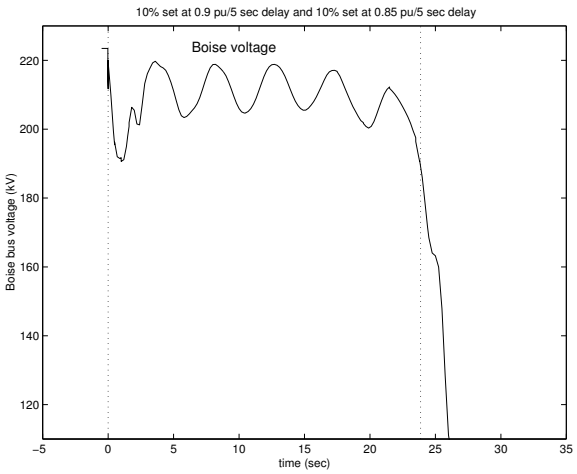

Figure 70. Boise voltage with Boise load shedding

2.3. Summary:

The analysis in this section shows that power-flow results can be used effectively for understanding voltage instability phenomena. The power-flow results are generally more conservative than the results from the dynamic simulations. However, they are mostly consistent in predicting voltage instability phenomena. Validated models of the dynamic simulations have been used together with power-flow studies for showing the reactive power shortages in the Idaho area during the July 2, 1996 which played the dominant role in causing the fast voltage collapse that led to the blackout. Modeling of exciter overcurrent limiters is important even in midterm (30 seconds) transient stability simulations when multiple contingencies are considered, especially under voltage stressed operating conditions. Detailed representation of load models is also important in dynamic models.

3. Analysis of August 10, 1996 blackout

The western system experienced a second major outage on August 10, 1996, while the study group was still investigating the causes of the July 2, 1996 blackout. Unlike the July 2, 1996 event wherein the separation was preceded by a fast voltage collapse, undamped oscillations of growing amplitude were seen across the entire western system prior to the system separation on August 10, 1996. A detailed summary of the line trippings and generator outages that occurred on August 10, 1996 can be seen in the NERC disturbance summary report [10] on pages 39 to 50.

At the start of the event, several key 500 kV transmission lines were out of service because of maintenance schedule as well as from relay actions. The voltages in Pacific Northwest were on the lower side because of heavy summer loading conditions. The main event itself started at 15:47:36 Pacific time with a fault on the 230 kV Ross-Lexington line near Portland, Oregon. The protective relays opened the line along with the neighboring 230 kV line Lexington-Woodland, and the small generating unit at Swift was also tripped. Subsequently, when the reactive power output of the MacNary generation units was at about 480 MVAR to provide reactive support, the protective relays started tripping the McNary units one by one because of faulty relay operation. As the McNary units went out of service, the interarea oscillations grew in magnitude, and the damping of the 0.25 COI interarea mode appeared to change from positive damping values to negative damping values. At 15:48:51, within 75 seconds after the initial fault on the Ross-Lexington line, the COI lines were tripped which resulted in system separation and the blackout.

In Section 3.1, we present the model validation efforts at WSU in duplicating the recorded system responses in computer model simulations. In Section 3.2, we will discuss a few sensitivity studies of the impacts of key switching events during the blackout. *We also show that the system operating condition was not dynamically secure at 15:47:36 in the sense that any one of many single contingencies could have resulted in the negatively damped oscillations of the 0.25 Hz mode.* The system was severely stressed at that time from previous outages of key 500 kV transmission lines, and the tie-line flow on the COI paths were higher than secure levels for guaranteeing N-1 security.

In Section 3.3, we carry out small-signal analysis of the validated model along the switching sequence of outages as they occurred during the blackout and show that the damping of the interarea 0.25 Hz mode indeed moved from positive damping values to negative damping values. In other words, the eigenvalue associated with the 0.25 Hz COI mode moved from open left half plane to the open right plane during the occurrence of the August 10, 1996 disturbance. *This shows that the western power system underwent a Hopf bifurcation on August 10, 1996 prior to system separation.* In Section 3.4, we study the nonlinear aspects of the Hopf bifurcation. We propose a novel method for tracking unstable limit cycles in large scale power system models. Using this method, we compute a bifurcation diagram for the validated power system model of the August 10, 1996 event and establish the interactions of stable and unstable limit cycles in determining the evolution of the trajectories. Using these studies, *the eventual collapse of the western system was likely caused by a global bifurcation called the cyclic fold bifurcation from the annihilation of a stable limit cycle with an unstable limit cycle [9].*

3.1. Dynamic model validation studies:

The power-flow case for representing the system conditions at the start of the disturbance at 15:47:36 was developed by WSCC, and all the dynamic studies presented in this section use this as the power-flow base case. As in the case of the July 2, 1996 simulations, the base case WSCC model that is normally used in WSCC planning studies showed none of the oscillation problems when dynamic simulations were carried out using the same switching sequence as they occurred during the August 10, 1996 event.

In order to match the simulated response with the recorded measurements, the following data modifications were incorporated:

1) Detailed dynamic models of the HVDC controls on the two DC lines, namely, Pacific DC Intertie (PDCI) and Intermountain Power Pool DC line (IPPDC), were included in the model. The significance of detailed HVDC models in the validation studies of the August 10 disturbance has been emphasized in [4]. We thank BPA for providing us with the detailed models for both PDCI and IPPDC which have been used in all our studies. In the July 2nd disturbance, the PDCI flow was not an important factor, whereas for August 10th event, the DC models were important in duplicating the system response [4].

2) Exciter limiters were added to several key generators in Pacific Northwest from our previous experience in the validation studies of the July 2nd event.

3) Induction motor load models were incorporated at several key load buses in the Pacific Northwest. This was again consistent with the studies for the July 2nd event.

4) Governors on all the thermal units were blocked as n the case of July 2nd studies.

5) Static load models were tuned to match the observed system damping level at the start of the event.

With the changes noted above, the dynamic simulations on ETMSP (Figures 71 to 79) closely matched the actual system recordings from the August 10, 96 event as shown below.

Figure 71 shows the time-plot of the Malin 500 kV bus from the model simulation (dashed in Figure 71), which closely follows the actual recording (shown as a solid plot in Figure 71) from the event. The COI 0.25 mode frequency and the phase match well with the actual recording during the progress of the event. During the later stages of the event, the actual system voltages collapsed faster than during the simulations. The load models need to be better represented under large voltage and frequency deviations in the system.

Figure 72 compares the COI tie-line active power flow from the simulation with the recording. Again, they match well. There appears to be a small difference about 20 MW in their initial values. Otherwise, the phase and frequency of the oscillations in the simulation follow their counterparts in the actual recording.

The role played by the PDCI controls in the evolution of the oscillations has been discussed previously in [4]. We note that the PDCI power-flow in the simulation (dashed plot in Figure 73) is reasonably consistent with the recorded values.

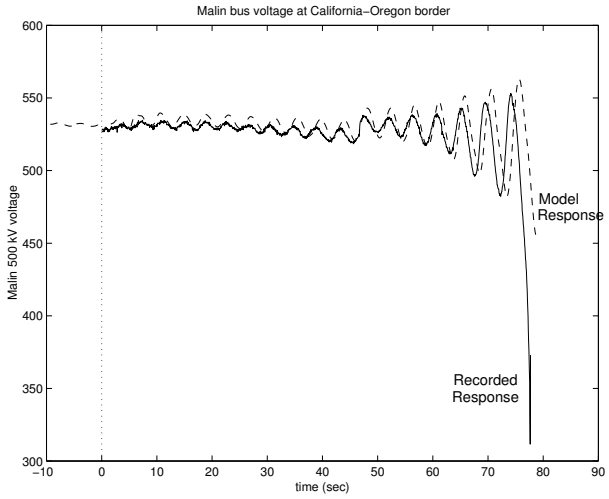

Figure 71. Malin voltage time-plot for the validated model

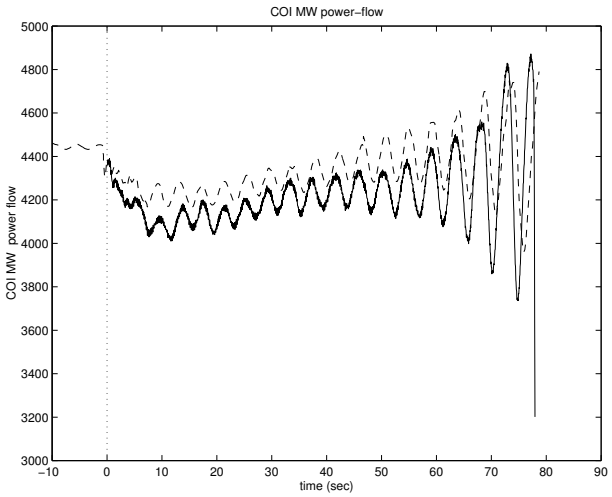

Figure 72. COI active power-flow for the validated model

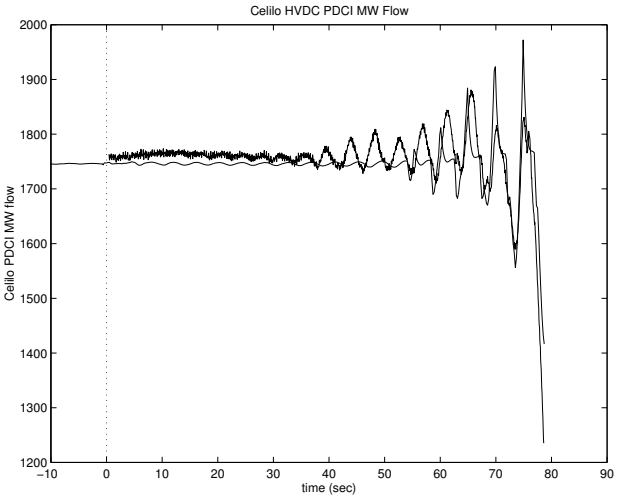

Figure 73. PDCI HVDC power-flow for the validated model

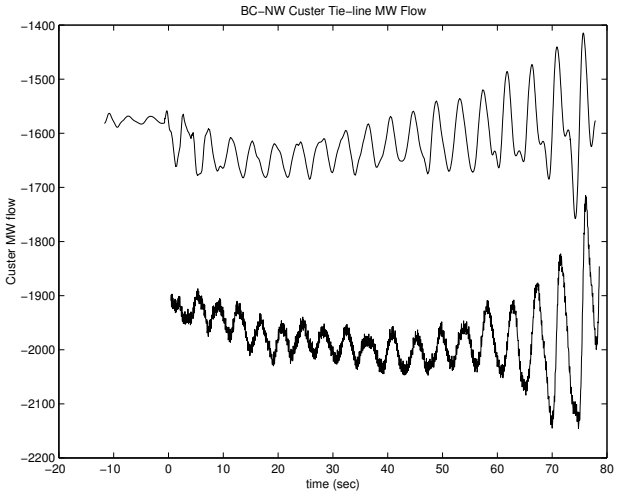

Figure 74. British Columbia to Northwest tie-line active power-flow

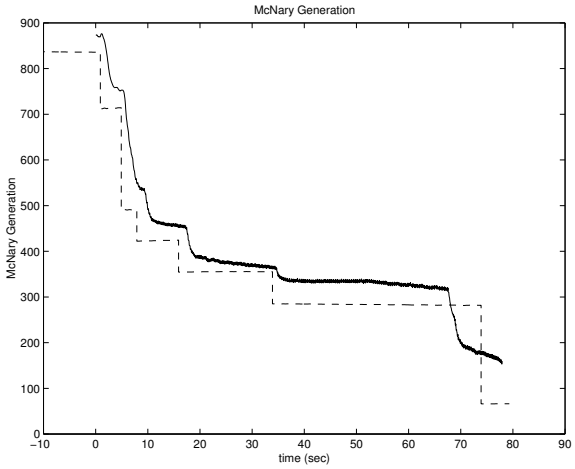

Figure 75. McNary generation for the validated model

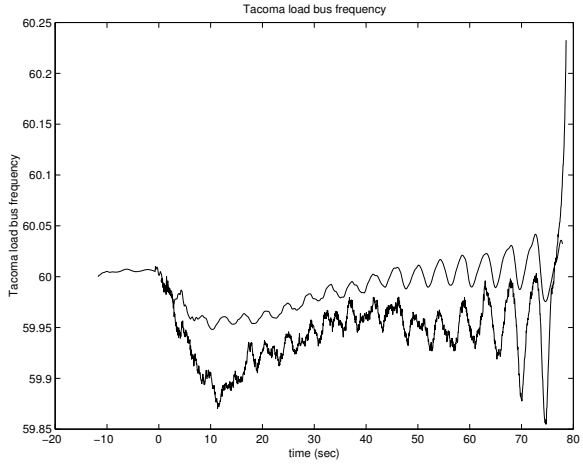

Figure 76. Tacoma load frequency for the validated model

Similarly, the tie-line active power-flow from British Columbia to Northwest (Figure 74) matches reasonably well, even though there are small mismatches in the initial values in the simulation.

Figure 75 shows the switching sequence followed for the tripping of the McNary units in the simulation which is consistent with the McNary power output during the event. The McNary plant was modeled in the form of several units which are tripped sequentially in the ETMSP simulation.

Figure 76 shows the load frequency behavior at the Tacoma load bus in the simulation as compared to the recorded response. The actual frequency dropped down to about 59.87 Hz at around 10 seconds after the start of the event, while the frequency only drops to about 59.94 Hz in the simulation. Later modeling efforts at BPA and in WSCC have addressed this issue by developing nonlinear governor models for the synchronous generators.

As a whole, we observe that the simulation model responses match reasonably well with the recorded responses during the entire sequence of events as they occurred during the August 10, 1996 disturbance. In the following sections, we will use this validated model for carrying out some sensitivity studies as well as for analysis of the small-signal; and nonlinear phenomena that affected the blackout event.

3.2. Sensitivity Studies:

We carry out two types of sensitivity studies in this section. First, we study the impact of switching events as they occurred during the disturbance. Let us define five switching scenarios as follows:

3.2.1. Snapshots of systsm status:

Case 0) Base case dynamic model: To study the damping level of the 0.25 Hz COI mode at the start of the event, we introduce a small disturbance, namely, open one of the COI lines and reclose it in 6 cycles. We did a Prony analysis [16] of the COI MW flow from the transient response and we estimated the damping of the COI mode to be +1.2% and the frequency to be 0.244 Hz. A more detailed discussion of the small-signal analysis follows in the next section 3.3.

Case 1) a) Trip the transmission line Ross 230 to Woodland 230, b) Trip the transmission line Lexington 230 to Woodland 230, c) Trip transmission line St John 115 to View Tap 115, and d) Disconnect Swift generator with 207 MW of generation. These four switchings occurred at the beginning of the disturbance at around 15:47 PDT. We start from the base case, and initiate these four switchings and carry out the dynamic simulation to study the status of the system at the end of these switching actions. Specifically, all the subsequent switching actions such as McNary trippings and AGC actions are suppressed. Our objective is to study the status of the

system if the subsequent switching actions had not taken place. The simulation is presented in Figures 77 and 78.

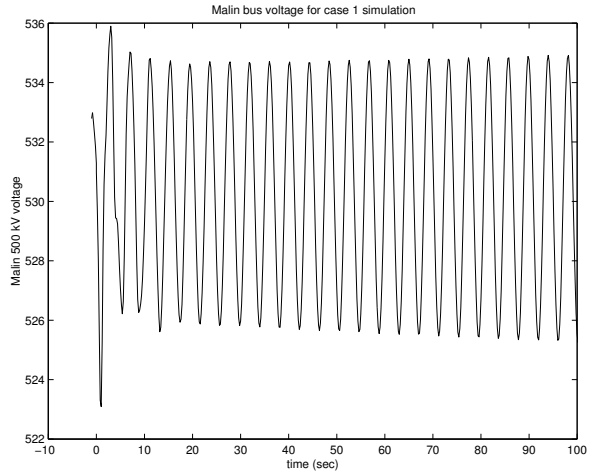

Figure 77. Malin voltage for Case 1 simulation

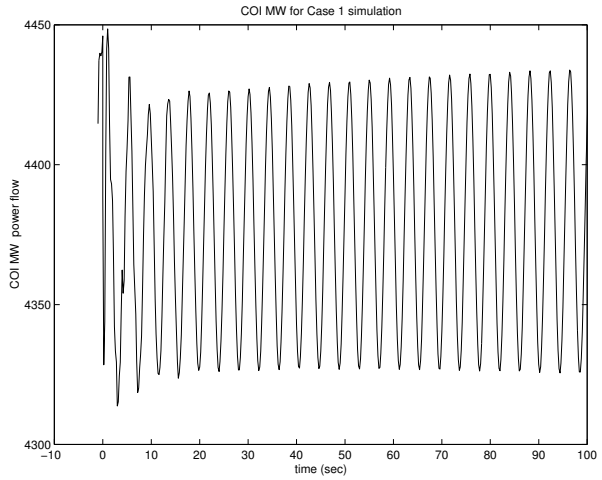

Figure 78. COI MW for Case 1 simulation

Both Figures 77 and 78 show that the damping of the COI 0.25 Hz mode to be near zero, and slightly negatively damped. Using Prony tool, we estimate the damping of the COI mode to be -0.1% and the frequency to be 0.242 Hz. We note that the four switching actions in the 230 kV circuit near Portland have contributed negatively to the damping of the COI mode shifting it from +1.2% to –0.1%. As such, these oscillations grow very slowly in magnitude and may not have resulted in severe consequences. Operators could have intervened in eliminating the oscillations by possibly reducing the COI tie-line flow or by switching in some capacitor banks.

Case 2) In addition to the trippings in Case 1, we switch out some of the McNary units, roughly amounting to a generation outage of 400 MW. Later switchings and AGC actions are not included. These actions roughly correspond to about 5 seconds after the start of the event. The simulation in Figures 79 and 80 shows the status of the system if the later McNary trippings and other actions had not taken place.

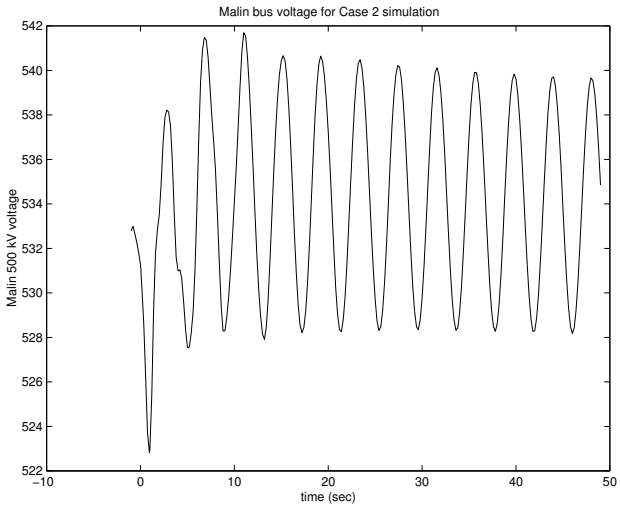

Figure 79. Malin voltage for Case 2 simulation

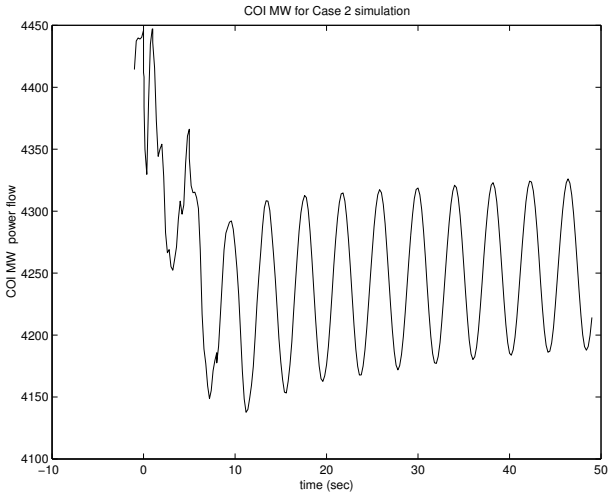

Figure 80. COI MW for Case 2 simulation

In Figures 79 and 80, the oscillations appear to be slightly positively damped. Prony analysis of the COI MW plot shows the damping of the 0.25 Hz mode to be at +0.1% and the frequency at 0.243 Hz. Tripping the McNary units reduces reactive power support in turn lowering the voltages. Lower voltages normally contribute negative damping to the 0.25 Hz interarea mode. However, the loss of McNary units have provided very small positive damping to the COI mode since the generation loss reduces the COI tie-line active power-flow. However, just like for Case 1, the oscillations are nearly undamped, and operator intervention would have been necessary to mitigate the oscillations. The AGC actions that followed the McNary trippings contributed significant negative damping to the 0.25 Hz mode.

Case 3) After the trippings in Case 2, a) disconnect more McNary units roughly amounting to additional 140 MW generation loss, b) model the AGC actions by ramping the outputs of Grand Coulee, John Day and Chief Jo by roughly 150 MW, 100 MW and 70 MW, respectively. These trippings

take the system to about 40 seconds after the initial 230 kV trippings, and latter actions are not included.

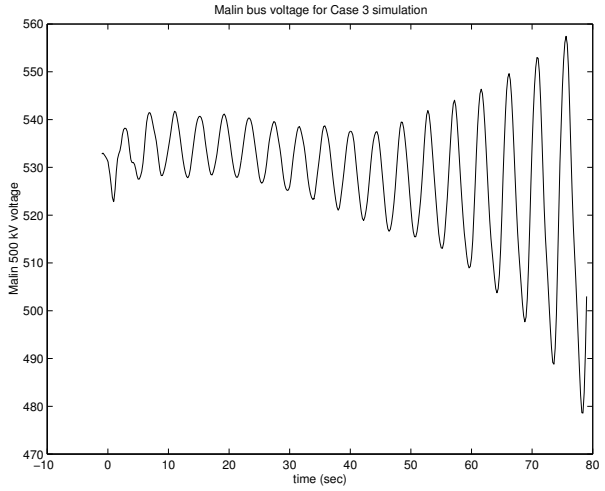

Figure 81. Malin voltage for Case 3 simulation

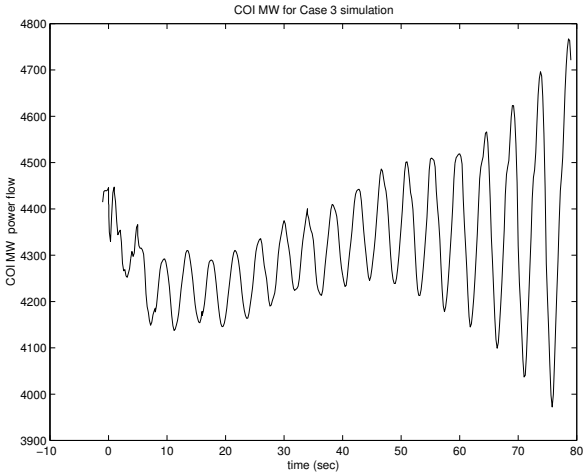

Figure 82. COI MW for Case 3 simulation

The simulations in Figures 81 and 82 already display the main characteristics of the August 10, 96 disturbance. The COI 0.25 Hz mode has become negatively damped, resulting in growing oscillations. As the oscillations become larger, the nonlinear effects contribute to faster growth of the oscillations. Prony analysis of the COI MW flow over the time-period from 20 to 40 seconds shows the damping of the 0.25 Hz mode at –1.6% and the frequency at 0.237 Hz.

<u>*Case 4)*</u> In addition to the trippings in Case 3, switch in Malin 200 MVAR capacitor bank, roughly at 50 seconds from the start of the disturbance. The simulations in Figure 83 and 84 show that the switching of the shunt capacitor bank at Malin did not contribute significant to the damping of the oscillations.

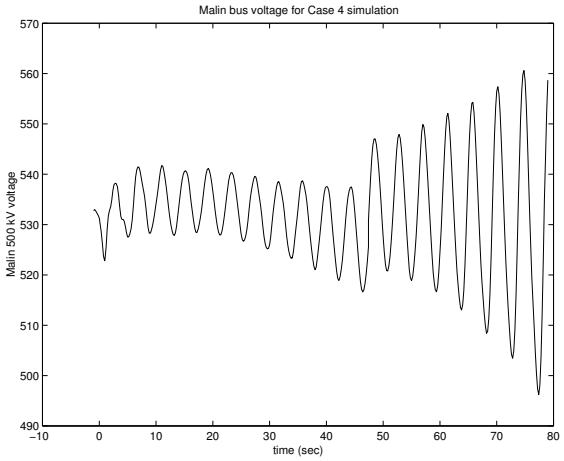

Figure 83. Malin voltage for Case 4 simulation

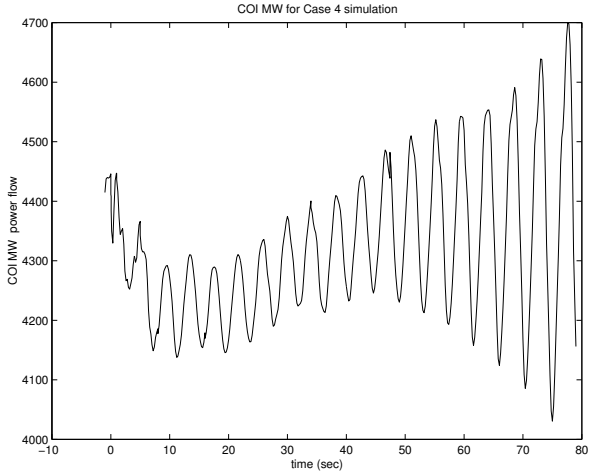

Figure 84. COI MW for Case 4 simulation

<u>*Case 5)*</u> Carry out all the switching actions as in the validated simulation model. The results were presented in the previous section.

In summary, it appears that the system was likely marginally damped (either positively or negatively) during the initial stages of the event. Later McNary trippings and AGC actions appear to have moved the 0.25 Hz mode well into the open right half complex plane, rendering the system small-signal unstable.

3.2.2. Contingency studies:

Few start with the base case power-flow and the validated dynamic data, and carry out specific contingency scenarios of 1) loss of one COI line, and 2) loss of all McNary units.
We will see that the system is unstable for the COI line single outage (hence, dynamically insecure), while it is stable for the McNary outage contingency.

3.2.2.1) Sensitivity to a single COI line outage:

We trip the line Captain Jack 500 to Grizzly 500 and simulate the contingency using the validating model. Figures 85 and 86 show that the damping of the 0.25 Hz interarea mode becomes negative following the single line outage, and the system would have experienced an outage similar to what occurred during the August 10, 1996. Therefore, the western system at the start of the disturbance at 15:47 was no dynamically secure with respect to first contingencies. Any one of many contingencies could have rendered the system unstable.

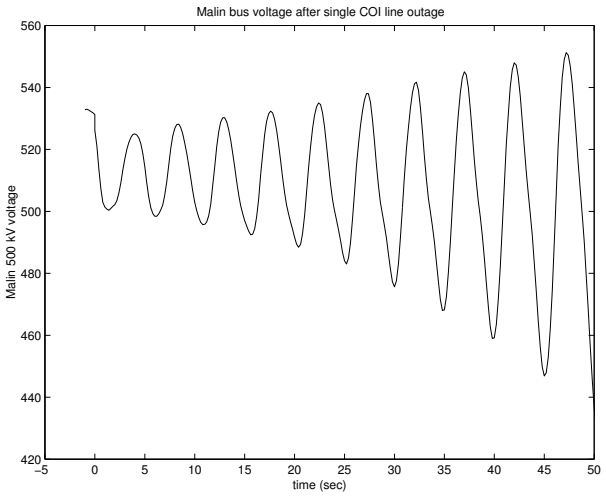

Figure 85. Malin voltage after single COI line outage

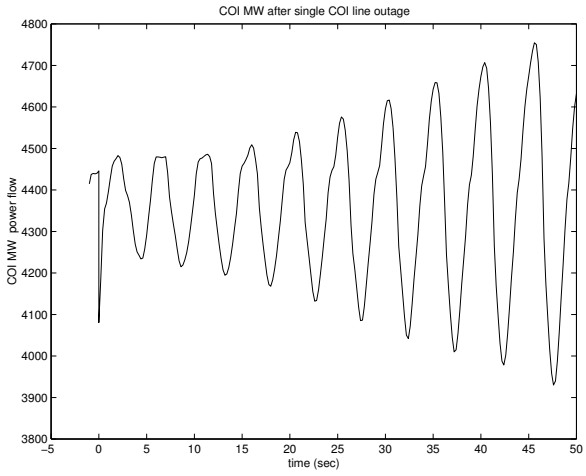

Figure 86. COI MW flow after single COI line outage

3.2.2.2. Sensitivity to McNary trippings:

For the validated model, we trip all the McNary units simultaneously and the simulation is shown in Figures 87 and 88. Prony analysis of the COI MW flow over the time interval 15 to 25 seconds shows the 0.25 Hz COI mode to have a damping of +1.6% with the frequency at 0.249 Hz. Comparing with the base case damping of +1.2% for the COI mode, we observe that the loss of all the McNary units by themselves would have provided very small positive damping to the COI mode, since the COI MW flow decreases with the generation loss. The positive contribution to damping from the reduction in COI transfer compensates for the negative contribution to damping from the loss of reactive support and lower voltages.

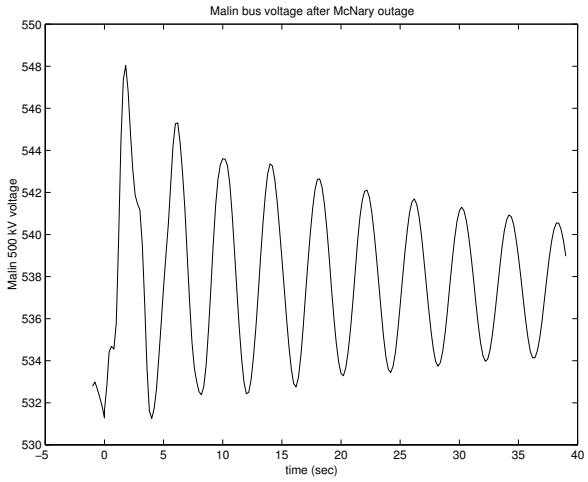

Figure 85. Malin voltage after a full McNary outage

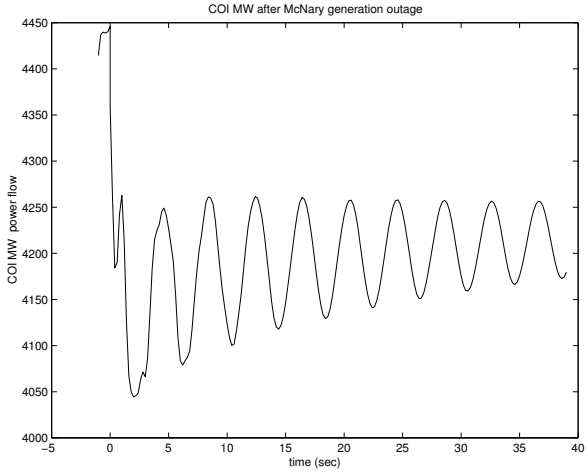

Figure 86. COI MW after a full McNary outage

3.2.2.3 Sensitivity to AGC actions:

In order to study the impact of AGC initiated generation increases at Grand Coulee, Chief Jo and John Day, we simulate the validated model by including the initial 230 kV line trippings and the Swift generation outage, and all the later McNary trippings. The AGC initiated generation changes and Malin capacitor bank insertion are not simulated. The simulations in Figures 87 and 88 show that the system was likely negatively damped at the end of McNary trippings with a small negative damping. Prony analysis shows the damping of the 0.25 Hz mode at –0.4% with the frequency at 0.249 Hz. It will take several minutes before such marginally negatively damped oscillations become a serious problem and operator intervention in the meantime could have mitigated the oscillations. Therefore, AGC initiated generation increases at Grand Coulee, John Day and Chief Jo significantly contributed

to the negative damping of the COI mode and to the fast break-up of the western system.

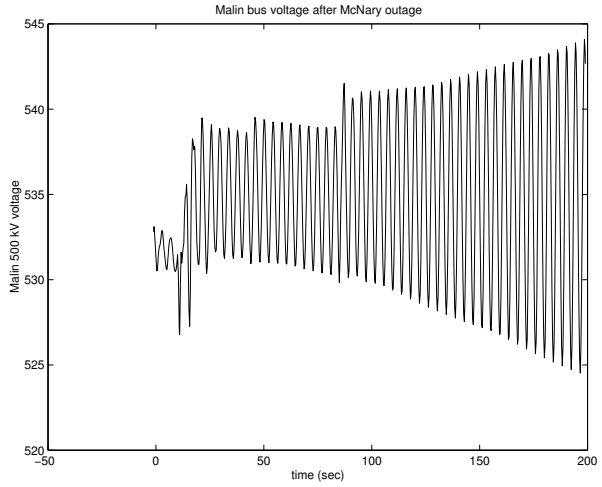

Figure 87. Malin voltage without the AGC actions

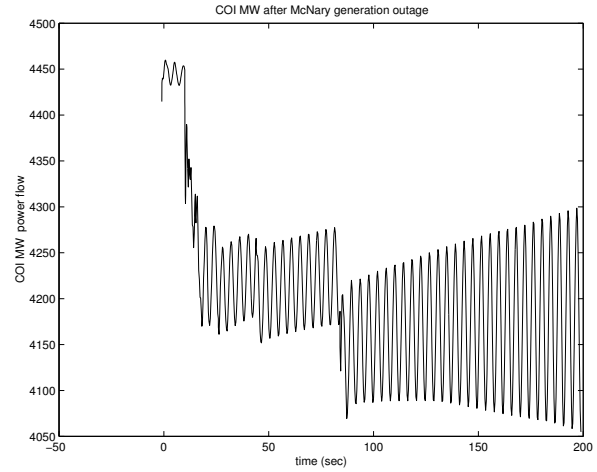

Figure 88. COI MW without the AGC actions

3.3. Small-signal analysis:

In this subsection, we will study the small-siganl stability properties of the system during the August 10, 96 event by taking power-flow snapshots of the system as it progressed through the switching actions. Nominally, the EPRI small-signal analysis program PEALS would have been the ideal candidate to carry out the eigenvalue analysis. However, after the detailed HVDC user defined models for the two DC links, PDCI and IPPDC, were included in the model, PEALS could not handle the large number of blocks in the detailed DC models. This resulted in error messages and unreliable damping estimation from the PEALS program.

As an alternative, we simulated small-disturbances for the different power-flow cases using the transient stability program ETMSP, and analyzed some of the system variables such as the COI MW flow using Prony for estimating the damping of the 0.25 Hz interarea mode. We opened a 500 kV line and reclosed within a few cycles to initiate a small disturbance. In our previous studies without the detailed HVDC models, the PEALS results matched well with the Prony analysis described above.

Small-signal stability is associated with an equilibrium condition of a power system. Since the system encountered several switching actions during the August 10, 96 event, we generated a set of power-flow cases that would roughly serve as power-flow snapshots at different instants during the disturbance. The power-flow cases are described below, and they are consistent with the transient simulations Cases 1 through 5 in Section 3.2.1.

Case 0): WSCC power flow system scenario at time 15:47:36 on August 10, 1996, just prior to the fault on the 230 kV line.

Case 1) (from Base Case)

a) Trip transmission line Ross 230 – Woodland 230;
b) Trip transmission line Lexington 230 – Woodland 230;
c) Trip transmission line St. John T 115 – View Tap 115;
d) Disconnect generator Swift 13.8, tripping 207 MW of generation.

Case 2) (from Case 1)

Disconnect some McNary units, tripping 414MW of generation.

Case 3) (from solved Case 2)

a) Disconnect more McNary units, tripping additional 138 MW of generation;
b) Increase generation of Coulee by 150 MW, John Day by 100 MW and Chief Jo by 70 MW to represent AGC actions following the generation trippings.

Case 4) (from Case 3)

Switch in Malin 200 MVAR cap bank.

Case 5) (from Case 4)

a) Disconnect rest of the McNary units, tripping 215 MW of generation;
b) Increase generation of Coulee by 50 MW, John Day by 50 MW and Chief Jo by 30 MW to account for AGC actions;

The system lost two key 500 kV lines shortly before the fault on the 230 kV line, and in order to study the impact of those two 500 kV lines, we also introduce a new case, called, Case –1 next.

Case -1) (From the base case)

Switch in two 500 KV transmission lines Allston to Keeler and Keeler to Pearl. (This was just before the disturbance of around time15:42:03).

Starting from the base case, the different power-flow scenarios are generated sequentially. In solving the different cases, we kept the COI transfer flow at the base case value so as to represent nominal equilibrium conditions for that configuration. Note that this assumption is different from the transient simulations in Section 3.2, wherein the COI MW flow changed dynamically following generation losses and subsequent governor actions.

For each of the power-flow cases, we estimated the damping of the COI 0.25 Hz mode using the Prony analysis and the results are first summarized in Table 1.

TABLE 1. BEHAVIOR OF THE 0.25 HZ COI MODE

Case	COI MW	Damping	Frequency (Hz)
-1	4419	+3.59%	0.2550
0	4411	+1.20%	0.2446
1	4409	-0.26%	0.2389
2	4409	-0.91%	0.2363
3	4409	-1.12%	0.2351
4	4413	-1.05%	0.2370
5	4414	-1.17%	0.2340

From Table 1, it is clear that the eigenvalue associated with the 0.25 Hz COI mode moves from open left half plane into open right half plane with the occurrence of the switching actions. Specifically, the system appears to undergo a Hopf bifurcation from Case 0 to Case 1. Also, the loss of the two 500 kV lines played a crucial role in reducing the damping of the 0.25 Hz mode from acceptable levels (above +3% in Case -1) to critically low levels (about +1% in Case 0). Also, the McNary trippings appeared to provide small positive damping in transient simulations because they resulted in an immediate reduction in COI active power-flow. Whereas in the power-flow cases here, we have maintained the COI flow at constant flow around 4400 MW in the spirit of steady state conditions. In this sense, the initial McNary trippings provide small negative damping to the 0.25 Hz mode. The later McNary trippings as well as the AGC actions contribute small negative damping to the 0.25 Hz mode. Malin shunt capacitor bank insertion provides very small positive damping to the mode.

In the small-signal analysis, the damping of the mode does not become significantly negative. In the real system as well as in transient simulations in Section 3.1, as the oscillations become larger, the nonlinearities in the system play a significant role in accelerating the divergence of negatively damped growing oscillations. This fact was previously noted and emphasized in [4].

However, based on the results in Table 1, *it is clear that the system has lost the small-signal stability at the equilibrium by undergoing a Hopf bifurcation.* This fact is nicely illustrated in Figure 89 by a root locus like diagram of the 0.25 Hz eigenvalue from Case –1 to Case 5. Methods for computing Hopf bifurcation boundaries in large system models have been proposed and tested in [17].

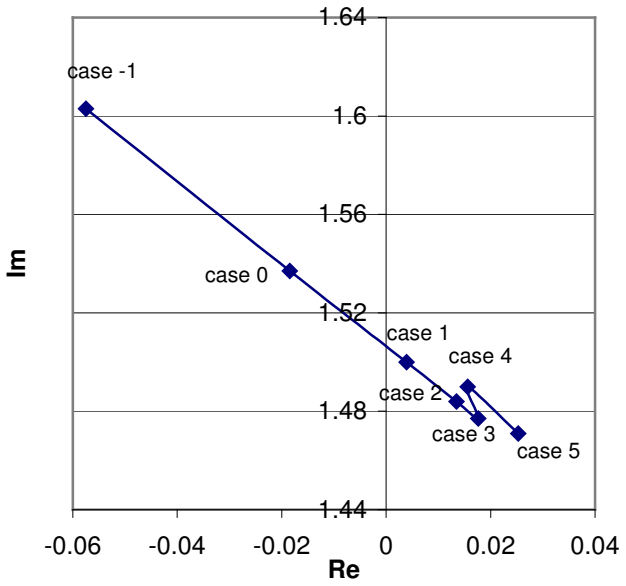

Figure 89. Locus of the 0.25 Hz mode eigenvalue from Case –1 to Case 5

Next, we consider the power-flow cases one by one. For each case, the steady state COI tie-line power-flow transfer from Northwest to California is varied by adjusting the slack bus generations in Northwest and California. We compute the damping of the 0.25 Hz mode for different COI MW flows and study the results. We will see that the damping of the 0.25 Hz mode normally decreases as the COI MW transfers get higher, and the system undergoes a Hopf bifurcation at some COI MW flow value. Therefore, the COI MW transfer can be used as the bifurcation parameter for studying the nature of the oscillations.

The eigenvalue locus for Case –1 is presented in Figure 90 as the COI MW export is varied from 4419 MW to 4966 MW. The Hopf bifurcation occurs at approximately 4860 MW for Case -1. In contrast, Hopf bifurcation occurs at the COI MW flow of 4570 MW for Case 0 in Figure 91. The values of Hopf bifurcations for Cases 1, 2, 3, 4, and 5 are respectively, 4385 MW, 4300 MW, 4280 MW, 4290 MW and 4230 MW in Figures 92, 93, 94, 95 and 96 respectively. (Details can be seen in the dissertation [9]).

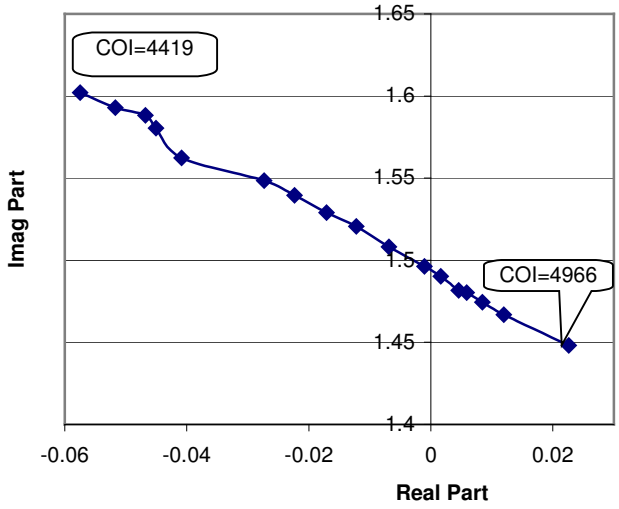

Figure 90. Eigenvalue locus for Case –1

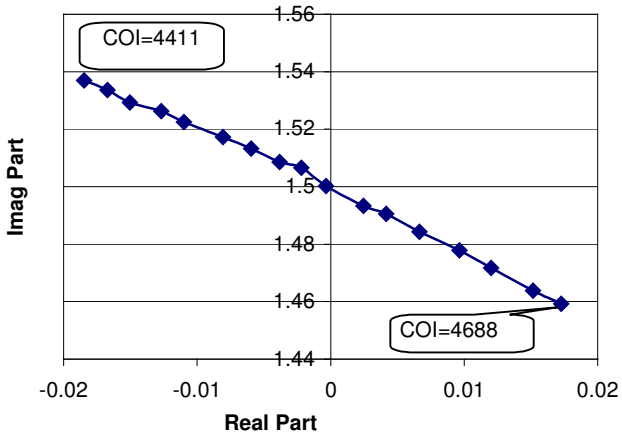

Figure 91. Eigenvalue locus for Case 0

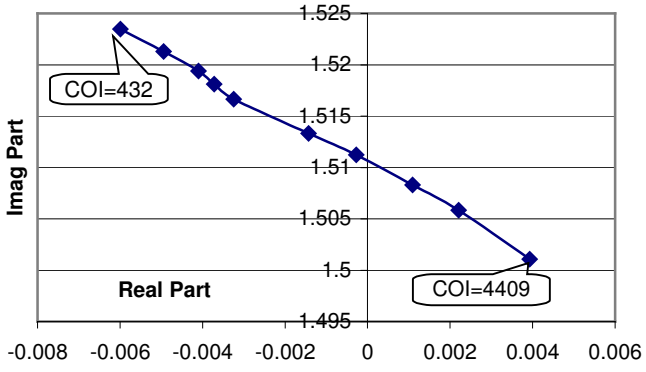

Figure 92. Eigenvalue locus for Case 1

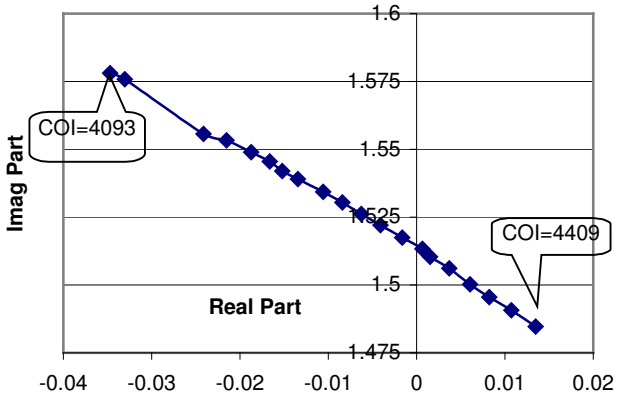

Figure 93. Eigenvalue locus for Case 2

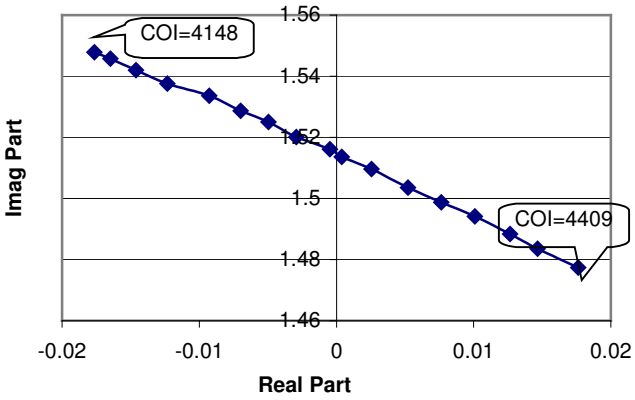

Figure 94. Eigenvalue locus for Case 3

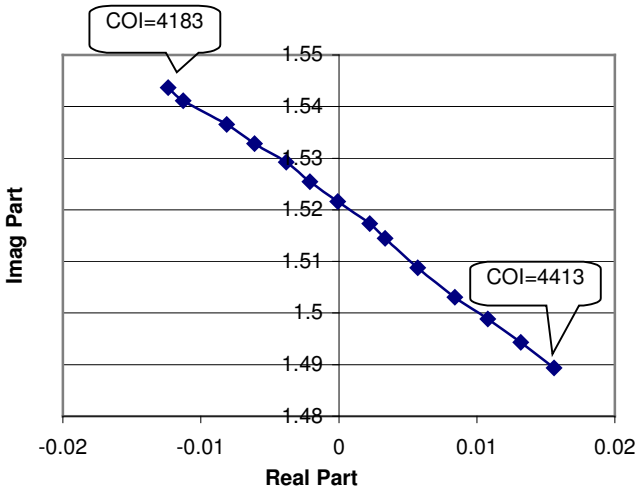

Figure 95. Eigenvalue locus for Case 4

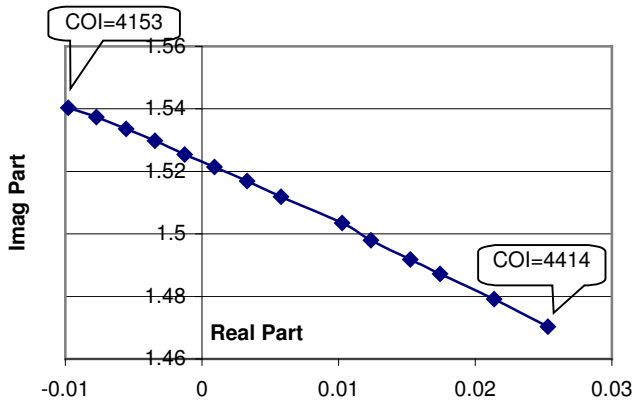

Figure 96. Eigenvalue locus for Case 5

In summary, the operating COI MW transfer of 4410 MW at the start of the August 10, 96 event (at 15:47 PDT) was well inside the Hopf bifurcation boundary value of 4860 MW for Case –1 before the loss of the two key 500 kV lines. The operating value of 4410 MW was close to the Hopf bifurcation limiting value of 4570 MW for the base case, Case 0, just prior to the fault on the 230 kV Ross line. With the tripping of the 230 kV lines and the Swift generator at 15:47 PDT, the operating value of 4410 MW for the COI transfer shifted outside the Hopf bifurcation boundary, an the system had undergone a Hopf bifurcation, resulting in a small-signal unstable equilibrium point according to our validated model of Section 3.1. As further switching actions occurred, the operating value was moving further and further away from the Hopf bifurcation values and the system was becoming "more" small-signal unstable, leading to fast diverging oscillations.

3.4. Nonlinear analysis of Hopf bifurcation phenomenon:

In this section, we will study the nonlinear implications of the Hopf bifurcation by using a novel method for tracking the unstable limit cycles.

3.4.1. A trajectory analysis method for finding unstable limit cycles:

Traditional methods for finding unstable limit cycles formulate the problem into finding the zeros of an associated discrete map (called the Poincare map [15]) , which requires order *n* numerical integrations of the trajectory for an *n* dimensional system. For very large systems such as the power system, such methods are clearly not applicable. In this section, we propose a new heuristic method for finding the interesting unstable limit cycles by carrying out a small number of numerical integrations.

Among the unstable limit cycles (ULC's) in a nonlinear system, the critical ones are those, which anchor the stability boundary of the region of attraction of the stable equilibrium point. Using nonlinear dynamical system theory, under some transversality conditions [6], it can be shown that the stable manifold[2] [6] of these unstable limit cycles will entirely belong to the stability boundary of the region of attraction. Among the ULC's on the stability boundary, the critical ones will be those with stable manifolds of dimension *n-1* for an *n*-dimensional system [6].

Let us focus on the neighborhood of the stable manifold of an ULC that we want to locate. The trajectories that originate inside the stable manifold of the ULC will then converge to the stable equilibrium point, while the ones that originate outside the stable manifold will diverge away. Accordingly, if we can find two initial conditions such that one lies inside the stable manifold of the ULC, and the other outside the stable manifold of the ULC, we can iterate between the two to get arbitrarily close to the stable manifold of the ULC. By definition, the trajectories on the stable manifold of the ULC approach the ULC. Therefore, *the iteration algorithm described above will approach arbitrarily close to the ULC on the stability boundary.* The details of the algorithm can be seen in the dissertation [9].

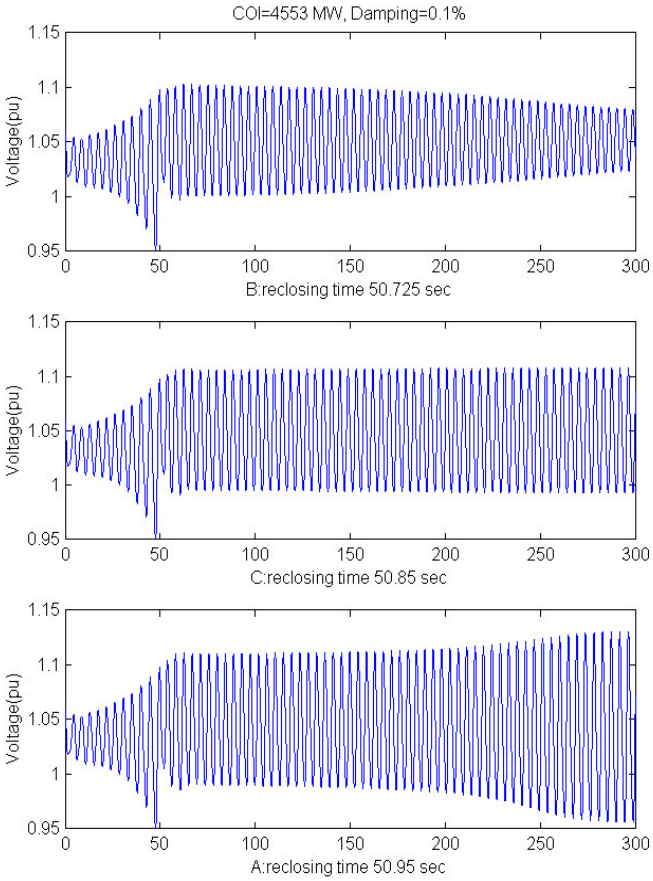

Figure 97. Illustration of the algorithm for finding ULC

[2] Roughly speaking, the stable manifold of an unstable limit cycle consists of all the trajectories that asymptotically converge to the unstable limit cycle.

Next, we will apply this technique for studying the nature of limit cycles associated with the Hopf bifurcations observed in Section 3.3. We focus on the base case power-flow Case 0, and we use the steady state COI MW transfer as the bifurcation parameter as in Section 3.3. Using the technique summarized above, in Figure 97, we illustrate an example of a ULC computed for COI MW transfer value 4553 MW, which corresponds to a damping of +0.1% for the 0.25 Hz COI mode.

In Figure 97, the first trajectory on the top is just inside the stable manifold of the ULC, and it converges to the stable equilibrium point. Contrastingly, the lowest trajectory is just outside the stable manifold of the ULC, and it results in slow oscillatory divergence. In the dissertation [9], an iterative algorithm is proposed that utilizes Unix shell programming for iterating the initial conditions between the top trajectory and the lower trajectory. The final converged solution is illustrated in the middle figure, wherein the trajectory is virtually on the stable manifold of the ULC. Thus, the trajectory in the middle plot of Figure 97 stays very near the ULC itself, displaying sustained oscillations. By using this method, we have computed the ULC for the bifurcation parameter value of COI MW transfer at 4553 MW.

The procedure is then repeated for different COI MW values, and a nice bifurcation diagram has been derived for the August 10, 1996 validated base case as shown in Figure 98. Interestingly, the WSCC system displays rich nonlinear properties near the Hopf bifurcation parameter value. The system has two different unstable limit cycles, as well as a stable limit cycle (SLC). The loci of the limit cycles are shown in Figure 98 using Malin bus voltage as the indicator of the size of the limit cycles. The locus of the equilibrium point is shown by the dotted line in the middle of the limit cycles.

In Figure 98, the system contains one unstable limit cycle of large amplitude that serves the anchor for the stability boundary of the ULC for COI MW values around 4500 MW. The size of the limit cycle is really large and the Malin 500 kV bus voltage fluctuates between 390 kV and 590 kV along this ULC. This large limit cycle is denoted the "outer ULC" in Figure 98.

A phase portrait of the ULC and the stable equilibrium point are shown in the plane of the COI MW flow and the Malin voltage magnitude in Figure 99 for the power-flow case with COI MW transfer at 4500 MW.

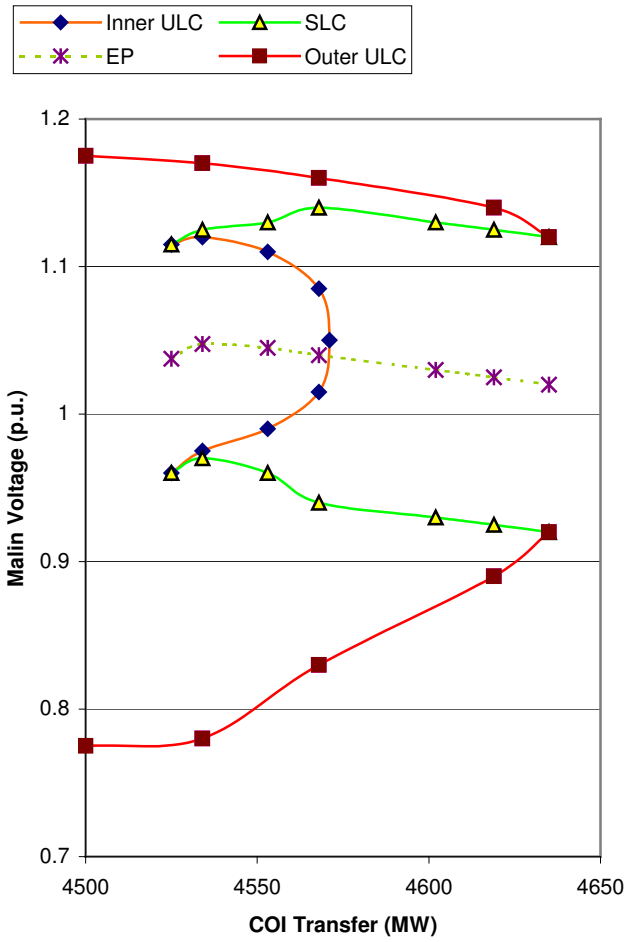

Figure 98. Bifurcation diagram

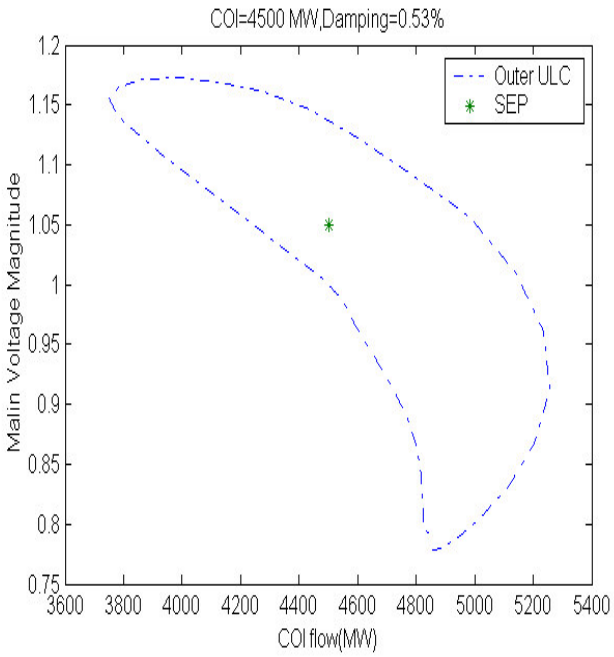

Figure 99. Phase portrait for COI transfer at 4500 MW

At around 4525 MW, the system undergoes a global bifurcation called the cyclic fold bifurcation [15] when a stable

limit cycle and unstable limit cycle are born simultaneously. This bifurcation is the limit cycle equivalent of the saddle node bifurcation (of the fold bifurcation) for equilibrium points. The stable limit cycle persists over a large range of COI MW transfer from 4525 MW to 4635 MW. The unstable limit cycle (called the "inner ULC" in Figure 98) shrinks in size as COI MW flows, and vanishes by moving into the equilibrium at the Hopf bifurcation value of 4570 MW. *The quadratic reduction in the size of the ULC as it approaches the Hopf bifurcation point is the classic indication of the occurrence of a subcritical Hopf bifurcation in the western system.*

For COI MW transfers between 4525 MW and 4570 MW, the system possesses two attractors, namely, the stable equilibrium point (SEP) (with marginally positive damping of the COI 0.25 Hz mode) and the stable limit cycle. An example is shown in Figure 100 for COI transfer at 4534 MW. Note that the regions of attraction for the stable equilibrium point and the SLC are separated by the stable manifold of the inner ULC.

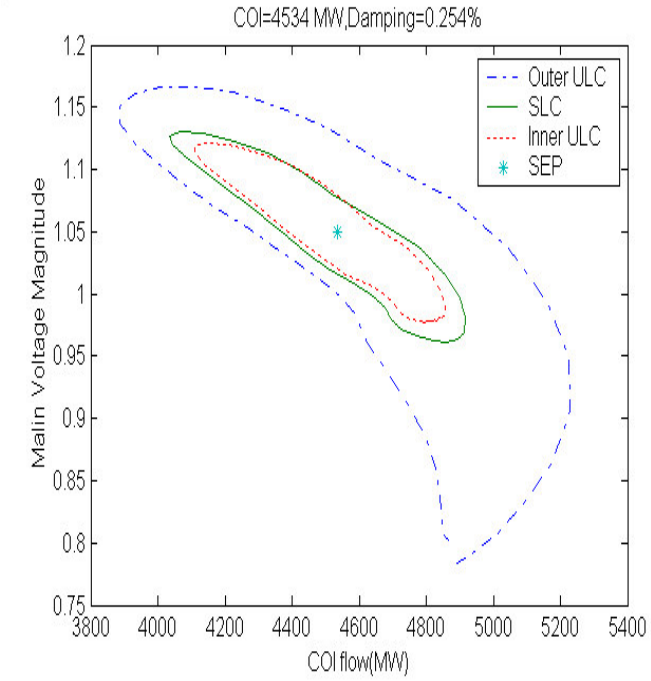

Figure 100. Phase portrait for COI transfer at 4534 MW

Figure 101 shows the phase portrait for COI transfer at 4568 MW that is close to the Hopf bifurcation point, and the inner ULC is moving closer to the SEP. Once the inner ULC shrinks onto the SEP, the small-signal stability of the equilibrium point is destroyed, leading to a small-signal unstable equilibrium point (UEP) for higher COI transfer values.

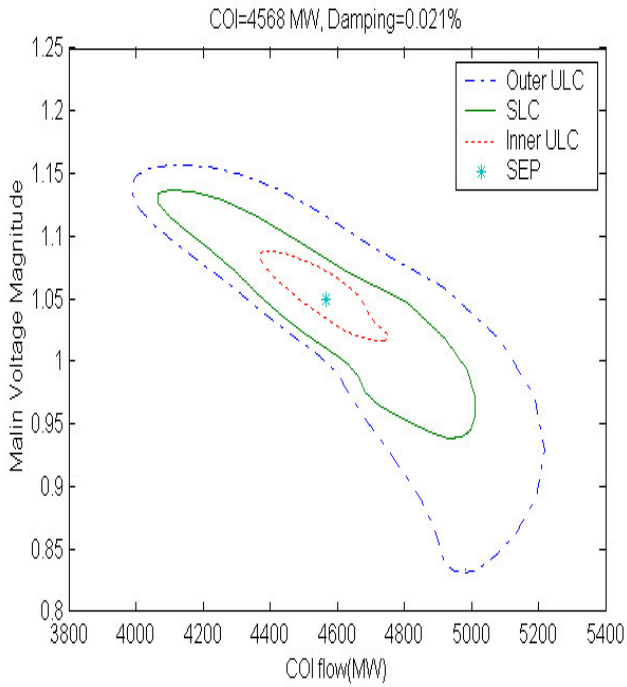

Figure 101. Phase portrait for COI transfer at 4568 MW

In Figure 102, the equilibrium point has become unstable after undergoing the Hopf bifurcation, and the trajectories diverging from the unstable equilibrium point (UEP) are captured by the stable limit cycle. In Figure 102, it can be seen that the outer ULC is quite close to the SLC, and even small perturbations can potentially push the system outside the stable manifold of the outer ULC, thus resulting in diverging oscillations.

At a parameter value of 4635 MW for the COI transfer, the system undergoes a reverse cyclic fold bifurcation in Figure 98. The SLC and ULC annihilate each other, rendering an absence of attractors for COI transfers above 4635 MW. Therefore, the outer ULC plays a crucial role in destroying the SLC so that all trajectories lead to oscillatory divergence for COI transfers above 4635 MW, just like the system response seen on August 10, 1996.

Even though the analysis has thus far been restricted to power-flow Case 0 in this subsection, we expect the bifurcation diagrams for other cases, Case 1 through Case 5, to be similar in nature. For COI transfers well above the Hopf bifurcation values, the absence of any attractor would imply oscillatory divergence of the trajectories as was observed during the August 10, 1996 event.

The bifurcation analysis presented in this subsection for the August 10, 1996 validated model of the WSCC power system shows that exotic nonlinear phenomena can occur even in realistic large-scale power system models. Moreover, they can also play significant roles in shaping the outcomes of large-scale events.

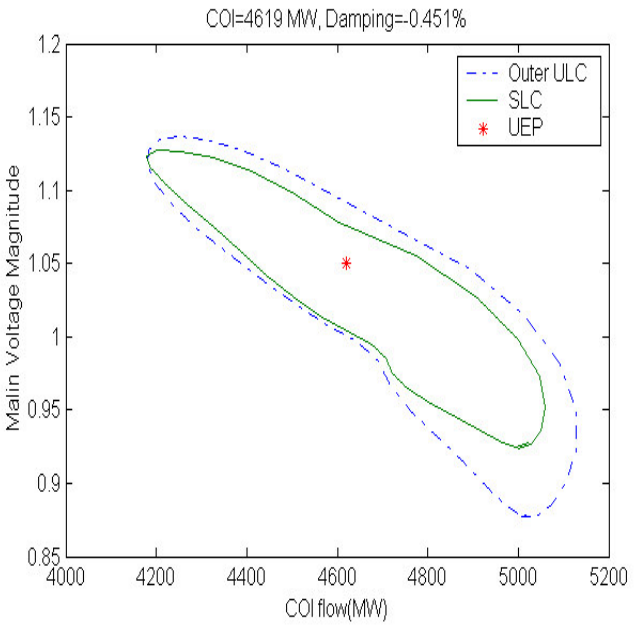

Figure 102. Phase portrait for COI transfer at 4619 MW

During the August 10, 1996 disturbance, the system recordings did display sustained oscillation like behavior for a time period of about 10 seconds. We also observed this in the sensitivity studies of Section 3.2. They could have been caused by near zero damping values of the COI 0.25 Hz mode at that time. It is also possible that the trajectory was close to either a stable limit cycle or an unstable limit cycle at that time. The presence of stable limit cycle near a small-signal unstable equilibrium point is especially useful in that the stable limit cycle can prevent growing negatively damped oscillations. However, for the validated model, the SLC exists over a small parametric window, and is quickly annihilated by another unstable limit cycle. The physical mechanisms behind the birth and annihilation of stable limit cycles in WSCC models need to be investigated.

Future research is suggested at developing other techniques for studying nonlinear phenomena in large-scale models so that we can derive valuable insight into the instability mechanisms of real power systems.

4. Conclusions

The paper has presented a detailed analysis of the validation studies and subsequent analysis of the validated models for the two blackout events that occurred in the summer of 1996 in the western power system. We have shown that the July 2, 1996 event was a voltage instability that was caused by the occurrence of a saddle node bifurcation. Power-flow studies showed that the system operation was rendered outside the static power-flow feasibility boundary by switching actions that occurred during the event. Dynamic studies indicated the occurrence of a dynamic saddle node bifurcation wherein the slow diverging trajectory (with a slow voltage decline) was accelerated by later tripping actions. The fast voltage decline at Boise and in the Northwestern system was likely caused the system approaching the singularity of the constrained model.

The August 10, 1996 event was on the other hand, a small-signal instability, wherein the eigenvalue associated with the 0.25 Hz COI interarea mode moved from open left half complex plane into the open right half complex plane by undergoing a Hopf bifurcation. Using a powerful method proposed here for tracking unstable limit cycles in large systems, we establish the Hopf bifurcation to be subcritical. Also, multiple unstable limit cycles as well stable limit cycles exist in the validated large scale model, and the interactions play crucial roles in determining the outcome of the trajectory near Hopf bifurcation parameter values.

Therefore, the analysis in this paper has clearly established the relevance of a) saddle mode bifurcations, b) Hopf bifurcations, c) singularity of the DAE models, d) unstable limit cycles, and d) global bifurcations for realistic large scale models. Further research is encouraged in applying the sophisticated nonlinear dynamic theoretic methods towards analysis and control of real power systems.

5. Acknowledgements

The first author thanks WSCC for his participation in the validation studies of the 96 blackouts that has largely contributed to this paper. All the opinions expressed in this paper are solely those of the authors. Specifically, the first author thanks Mr. Ron Schellberg at Idaho Power and Mr. Ravi Aggarwal at Bonneville Power Administration (BPA) for their help with the July 2, 1996 simulations. The author also thanks Dr. Kip Morrison and Mr. S. Yirga at Powertech Labs, BC, Canada, and Dr. Dmitry Kosterev and Dr. Bill Mittelstadt at BPA for their help with the August 10, 1996 simulations. And, the author expresses a special note of thanks to Mr. Carson Taylor at BPA for his consistent support and help in doing this work. The author also thanks the members of the WSCC OCSG group, many engineers from western utilities, who participated in the OCSG discussions on the blackouts.

This work was supported by NSF under the grants ECS-9320041 and ECS-9457126. Partial funding of the work from Bonneville Power Administration is also gratefully acknowledged. Additional funding from Power Systems Engineering Research Center (PSerc), and by Consortium for Reliability Technology Solutions (CERTS), funded by the Assistant Secretary of Energy Efficiency and Renewable Energy, Office of Distributed Energy and Electricty Reliability, Transmision Reliability Program of the U.S. Department of Energy under Interagency Agreement No. DE-AI-99EE35075 with the National Science Foundation.

6. References

[1] D. Kosterev, S. Yirga, and V. Venkatasubramanian, *Validation report of the August 10, 1996 WSCC disturbance*, Operating Capability Study Group, Western Systems Coordinating Council, March 1997.

[2] R. Aggarwal, R. Daschmans, R. Schellberg, V. Venkatasubramanian, and S. Yirga, *Validation studies of the July 2, 1996 WSCC system disturbance event*, Operating Capability Study Group, Western Systems Coordinating Council, July 1997.

[3] C.W.Taylor and D.C.Erickson, "Recording and analyzing the July 2 cascading outage", *IEEE Computer Applications in Power*, Vol. 14, Issue 1, January 1997, pp. 26-30.

[4] D. N. Kosterev, C.W.Taylor, and W.A.Mittelstadt, "Model Validation for the August 10, 1996 western system outage", *IEEE Trans. Power Systems*, Vol. 14, pp. 967-979.

[5] EPRI Final Report TR-108256, *System disturbance stability studies for Western System Coordinating Council (WSCC),* Sepetmber 1997, prepared by Powertech Labs, BC, Canada.

[6] V. Venkatasubramanian, H. Schattler and J. Zaborszky, "A Taxonomy of the Dynamics of a large Electric Power System with Emphasis on its Voltage Stability", *Proc. NSF International Workshop on Bulk Power Voltage Phenomena*, Maryland, August, 1991, pp. 9 - 52.

[7] D. J. Hill and I.M.Y.Mareels, "Stability theory for differential-algebraic systems with applications to power systms", *IEEE Trans. Circuits and Systems*, Nov. 1990, pp. 1416-1423.

[8] V. Venkatasubramanian, H. Schattler and J. Zaborszky, "A taxonomy of the dynamics of large differential-algebraic systems", *Proceedings of the IEEE,* November 1995, Vol. 83, No. 11, pp. 1530--1561.

[9] Yuan Li, *Coordination of transmission path transfers in large electric power systems*, Ph.D. Dissertation, School of Electrical Engineering and Computer Science, Washington State University, Pullman, WA, December 2003.

[10] 1996 System Disturbances, North American Electric Reliability Council, at
ftp://www.nerc.com/pub/sys/all_updl/oc/dawg/disturb96.pdf

[11] J. Jargis and F.D.Galiana, "Quantitative analysis of steady state stability in power networks", *IEEE Trans. Power Systems*, Vol. PAS-100, No.1, Jan. 1981, pp. 318-326.

[12] H.G.Kwatny, A.K.Pasrija, and L.Y.Bahar, "Static bifurcations in electric power systems: loss of steady state stability and voltage collapse", IEEE Trans. Circuits and Systems, Vol. CAS-33, October 1986, pp. 981-991.

[13] P. Kundur, *Power system stability and control*, McGraw-Hill, 1994.

[14] I. Dobson and H.D. Chiang, "Toward a theory of voltage collapse in electric power systems", *Systems and Control Letters*, Vol. 13, 1989, pp. 253-262.

[15] J. Guckenheimer and P. Holmes, *Nonlinear oscillations, Dynamical systems and Bifurcations of vector fields*, Springer-Verlag, 1983.

[16] J. F. Hauer, "Applications of Prony analysis to the determination of modal content and equivalent models for measured power system response", *IEEE Trans. Power Systems*, Vol. 6, No. 3, August 1995, pp. 1302-1313.

[17] K. Kim, H. Schattler, J. Zaborszky, V. Venkatasubramanian, and P. Hirsch, "Methods for calculating oscillations in large scale power systems", *IEEE Transactions on Power Systems*, November 1997, Vol.12, No.4, pp.1639-1648.